

Strategies for the Fabrication of Porous Platinum Electrodes

Arne Kloke, Felix von Stetten, Roland Zengerle, and Sven Kerzenmacher*

Porous platinum is of high technological importance due to its various applications in fuel cells, sensors, stimulation electrodes, mechanical actuators and catalysis in general. Based on a discussion of the general principles behind the reduction of platinum salts and corresponding deposition processes this article discusses techniques available for platinum electrode fabrication. The numerous, different strategies available to fabricate platinum electrodes are reviewed and discussed in the context of their tuning parameters, strengths and weaknesses. These strategies comprise bottom-up approaches as well as top-down approaches. In bottom-up approaches nanoparticles are synthesized in a first step by chemical, photochemical or sonochemical means followed by an electrode formation step by e.g. thin film technology or network formation to create a contiguous and conducting solid electrode structure. In top-down approaches fabrication starts with an already conductive electrode substrate. Corresponding strategies enable the fabrication of substrate-based electrodes by e.g. electrodeposition or the fabrication of self-supporting electrodes by dealloying. As a further top-down strategy, this review describes methods to decorate porous metals other than platinum with a surface layer of platinum. This way, fabrication methods not performable with platinum can be applied to the fabrication of platinum electrodes with the special benefit of low platinum consumption.

1. Introduction

The synthesis of porous platinum and the fabrication of porous platinum electrodes have attracted great attention during the last years since porous platinum brings together the high specific catalytic activity of platinum and a high surface area. Accordingly porous platinum is frequently used in chemical engineering for many organic reactions such as hydrogenations, refining of petroleum and in automotive exhausts.^[1–7] Porous platinum electrodes (electrocatalysts) are applied in various types of fuel cells,^[8–12] metal-air batteries,^[13,14] electrochemical

sensors,^[15–21] neural stimulation^[22–25] and mechanical actuators^[26] as further outlined in the section 1.1. Such porous platinum electrodes are characterized by an electrically conductive and contiguous electrode structure. Their surface either consists of pure platinum or platinum alloys. Their high surface area arises from an extended network of pores inside the electrode compound.

1.1. Applications of Porous Platinum Electrodes

In *fuel cells* porous platinum serves as catalyst for the electro-oxidation of fuels such as hydrogen, methanol, ethanol, formic acid or glucose as well as the electroreduction of oxygen.^[9,11,27–31] This is because platinum shows the highest catalytic activities of all pure metals for the corresponding reactions.^[10,12] The high surface area of porous platinum enables a high fuel turnover rate at low electrode polarization and hence a high power output of the fuel cell. A big drawback of platinum

is its price. The price of one ounce has increased from \$583 in 2000 to \$1581 in 2010.^[32] Therefore a main goal in fuel cell research is to reduce the mass of platinum per surface area during fabrication. One strategy to minimize the amount of platinum is to control the size and shape of the deposited structures.^[33] Control over size is important since for instance decreasing diameters enable an increasing surface to volume ratio and thus increasing numbers of catalytically active sites per mass which means higher platinum utilization (^[34], see Section 3.1.1). Moreover, control over microscopic shape is of particular interest since different crystallographic planes of platinum show different catalytic activities.^[31] Another strategy is to replace a fraction of platinum by a cheaper element such as ruthenium.^[35–37] In many fuel cell systems the application of alloy catalysts is also desired due to further reasons: For instance in methanol fuel cells alloy catalysts show a better resistance towards CO poisoning at the anode^[35,38–40] and an improved tolerance towards methanol crossover effects at the cathode^[27] compared to pure platinum.

Porous platinum electrodes are also applied in *electrochemical detection* of glucose,^[16,17,41–44] pH,^[45] dissolved oxygen,^[46] hydrogen peroxide,^[47–49] hydrogen^[20] or further gasses.^[21,50] In particular enzyme-free amperometric detection of glucose in physiological environments represents a challenging application

A. Kloke, Dr. F. von Stetten, Prof. R. Zengerle, Dr. S. Kerzenmacher
Laboratory for MEMS Applications
Department of Microsystems Engineering–IMTEK
University of Freiburg
Georges-Koehler-Allee 106
79110 Freiburg, Germany
Fax: (+49) 761 203 7322
E-mail: kerzenma@imtek.uni-freiburg.de
Prof. R. Zengerle
BIOSS Centre for Biological Signalling Studies
Albert-Ludwigs-Universität Freiburg

DOI: 10.1002/adma.201102182

in which the porosity plays an important role.^[16,17,41–43] Here, increasing signal selectivity for glucose oxidation compared to signals of interfering substances is obtained at increasing surface roughness.^[16,17] Similar observations are known from *implantable glucose fuel cells*.^[51–53] Here the high surface roughness can be utilized to promote the anodic glucose oxidation compared to the simultaneously proceeding cathodic oxygen reduction.^[51,52] With a significantly higher surface roughness at the anode compared to at the cathode, membrane-less fuel cells can be operated with the same catalyst material at anode and cathode in one solution containing both reactants dissolved oxygen and glucose.

In *neural stimulation* the signal to noise ratio can be improved by reducing the impedance of the implant-tissue interface. Since the impedance is inversely proportional to the effective surface area, high surface area electrodes such as platinum-black can be applied to increase signal quality.^[22–25] Another reason for choosing platinum in electrode material for neural stimulation arrays and other implantable electrode applications is because platinum is very noble and thus features high biocompatibility and chemical stability.

In *dye-sensitized solar cells* platinum electrodes are applied as counter electrodes since they combine high catalytic activity for the triiodide reduction and high electrical conductivity.^[54–59] Here nanoporous platinum electrodes fabricated by e.g. electrodeposition, electroless deposition or thermal decomposition are investigated to overcome the drawbacks of state of the art fabrication by sputtering or thermal evaporation technology. For instance the use of nanoporous electrodes lead to significant cost reduction due to their high surface to mass ratio the required amount of platinum is significantly reduced compared to state of the art.^[57] Moreover the corresponding fabrication techniques feature less operational costs and enable an improved optical transparency.^[55,57,58] Equal conversion efficiencies are reported for dye sensitized solar cells with sputtered and nanoporous counter electrodes.^[55,58,60]

1.2. Fabrication Strategies

According to **Figure 1** four general fabrication strategies can be distinguished: *nanoparticle-based* (Section 3), *substrate-based* (Section 4), *dealloying* (Section 5: *self-supporting electrodes*) and *decoration* (Section 6). *Nanoparticle-based fabrication* is a *bottom-up approach* to porous platinum electrodes: first a catalyst particle is generated and subsequently integrated into a solid electrode structure. In contrast to this the fabrication of *substrate-based* and *self-supporting electrodes* represent *top-down approaches*: The fabrication of *substrate-based electrodes* starts from a contiguous substrate structure and catalytic sites are created on top of it during fabrication. The fabrication of *self-supporting electrodes* by means of *dealloying* also starts from a contiguous structure, but different to in *substrate-based electrodes* the catalytic surface area is created inside of this structure. *Decoration* of non-platinum porous metals is a further top-down approach. Here an already highly porous structure is decorated by a thin layer of platinum.

In literature, several review articles exist discussing specific topics related to porous platinum such as nanoparticle



application in implantable glucose fuel cells.

Arne Kloke studied Interdisciplinary Science at the Swiss Federal Institute of Technology (ETH) Zürich, where he wrote his diploma thesis on organic semiconductors. In 2007 he joined the Laboratory for MEMS Applications at the Department of Microsystems Engineering - IMTEK, University of Freiburg. Here, his work has been focused on high surface-area platinum electrodes for



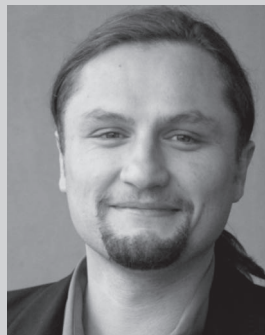
Today he heads the joint lab-on-a-chip research division of IMTEK and the Institut für Mikro- und Informationstechnik of the Hahn-Schickard-Gesellschaft (HSG-IMIT) in Freiburg.

Dr. Felix von Stetten studied Agricultural Engineering and Biotechnology at the Technical University of Munich, Germany, where he received his PhD in microbiology in 1999. After a three-year period of industrial research he joined the Laboratory for MEMS Applications at IMTEK, University of Freiburg, where he became involved in biofuel-cell and lab-on-a-chip research.



focused on lab-on-a-chip systems, nanoliter and picoliter dispensing, drug delivery systems, and biofuel cells.

Prof. Dr. Roland Zengerle is professor at the Department of Microsystems Engineering (IMTEK) and vice-chairman of the Center on "Biological Signalling Studies" at the University of Freiburg. He is director at the Institut für Mikro- und Informationstechnik of the Hahn-Schickard-Gesellschaft (HSG-IMIT) and European editor of the Springer Journal of Microfluidics and Nanofluidics. His research is



his main research interests are material and design aspects of enzymatic and microbial fuel cells.

Dr. Sven Kerzenmacher is heading the Biofuel Cell research group at the Laboratory for MEMS Applications, Department of Microsystems Engineering—IMTEK, University of Freiburg. He holds a Master Degree in Energy Conversion & Management and received his PhD in Microsystems Engineering from the University of Freiburg in 2010. In addition to implantable fuel cells and electrodes based on porous platinum,

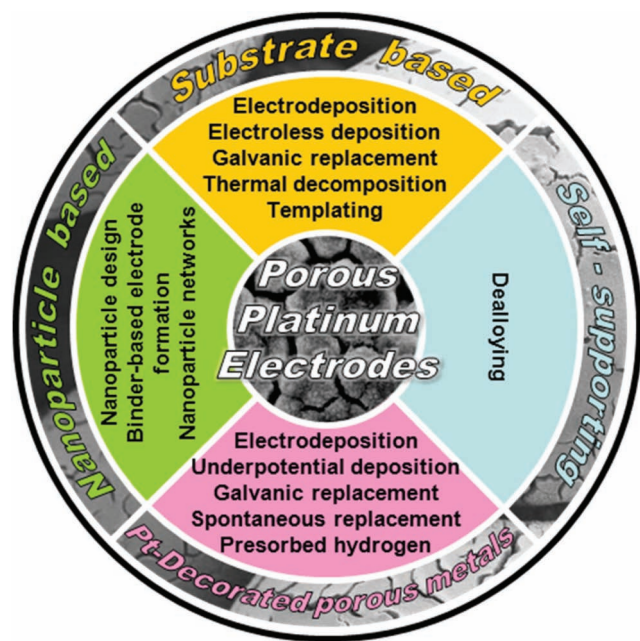


Figure 1. Classification of strategies enabling the fabrication of porous platinum electrodes.

synthesis,^[33,34,61–64] specific reduction methods^[65–67] or fabrication of PEM-FC electrodes^[68–70] or hydrogen sensors.^[20] A more general review on porous platinum materials has recently been published by Chen and Holt-Hindle, showing a selection of fabrication techniques and discusses structural, catalytic, optical and magnetic properties as well as application of such porous platinum structures.^[71] In this article we in detail review methods suitable to the fabrication of porous platinum electrodes as for instance required in fuel cell or sensor applications. For a deeper understanding of porous platinum structure formation Section 2 deals with reduction, deposition and particle formation from a more fundamental point of view. Sections 3–6 discuss fabrication approaches by their basic ideas, strengths and weaknesses, classified according to Figure 1. Finally an overall comparison of the strategies is carried out in the “conclusion” Section.

2. General Principles Behind the Deposition of Platinum

Porous platinum is in most cases obtained by either chemical or electrochemical reduction of commercially available platinum salts which therefore are also often described as *precursors*. Most prominent platinum salts are the four- and two-valent chloride-complexes hexachloroplatinate $[\text{PtCl}_6]^{2-}$ and tetrachloroplatinate $[\text{PtCl}_4]^{2-}$, respectively. Besides these chloride salts there are for instance tetraammine platinum nitrate $\text{Pt}(\text{NH}_3)(\text{NO}_3)_2$, diammine platinum nitrite $(\text{NH}_4)_2\text{Pt}(\text{NO}_2)_2$ as well as the metal-organic precursors such as platinum acetylacetonate $(\text{Pt}(\text{acac})_2)$, platinum dimethylcyclooctadiene. The following two subSections summarize the basic principles underlying

platinum deposition by *electrochemical and chemical reduction* pointing out their similarities and specific features. Alternative reduction pathways are summarized in Section 2.3.

2.1. Electrochemical Reduction

During electrodeposition platinum ions are electrochemically reduced to solid-state platinum and thus get deposited at the cathode (see Figure 2A). “Electrochemically reduced” means that the electrons required for this reduction are transferred to the platinum ions from the cathode (working electrode) and an external power supply (control unit for current or potential control), respectively. A deposition of platinum occurs if the cathode potential E_{cath} is more negative than the redox-potential of the according redox reaction. Electrodeposition can be used for the fabrication of porous catalysts (see Section 4.1, 4.2, 6.1) as well as for the deposition of smooth coatings required for decorative purpose or corrosion protection.^[65] Smooth crystalline layers of up to a thickness of 20 μm have been deposited from $(\text{NH}_4)_2\text{PtCl}_6$.^[65,72]

Electrodeposition is usually performed in a three electrode assembly at constant current (galvanostatic) or constant potential (potentiostatic) as shown in Figure 2A. Controlling the deposition current has the advantage of a linear relation between deposited charge and time with the drawback of a non-constant deposition potential. Hence the overpotential changes leading to variations in the reaction mechanism during deposition.

For a potentiostatic deposition a reference electrode is required to control the cathode potential. For a galvanostatic deposition a reference electrode is not essential. In deposition of metals like copper, zinc or others a block of the corresponding metal is used as dissolving counter electrode. This way a constant concentration of the metal salt in the electrolyte is automatically guaranteed.^[73] In case of platinum this is not possible due to the very high overpotential of electrochemical dissolution of platinum. This has two effects: First, the *precursor* concentration in the electrolyte decreases during deposition if no *precursor* addition is applied from an external source. Second, side reactions occur at the counter electrode (platinum in most cases) which can affect experimental conditions such as pH.

Since platinum ions are present in solution as complex ions the electrochemical reduction at the cathode proceeds in three consecutive steps^[65,73]

- 1 Transport of complexed platinum ions from the bulk solution to the cathode interface. This mass transport is driven by diffusive and if present convective forces.
- 2 Expression of the *electroactive species* in the electric field by removal of the ligands or other transformations of the complexed platinum ion. The *electroactive species* does not necessarily have to be the pure platinum ion, but can also be a complex ion.
- 3 Electron transfer from the cathode to the *electroactive species*.

Either of these three steps can be the rate determining step. For instance, a slow mass transport or a very strong ligand-platinum interaction can reduce the available concentration of

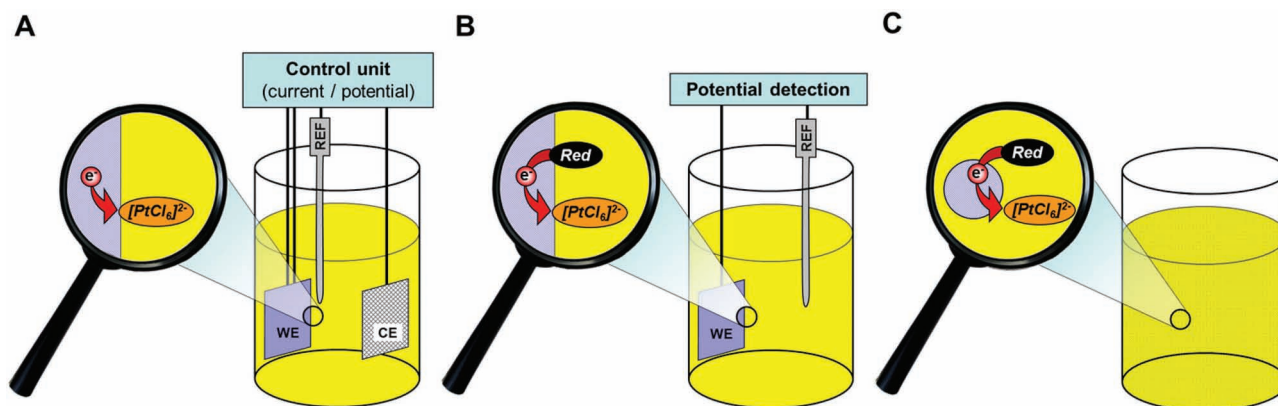


Figure 2. Typical setups and wire connections used for deposition of platinum by (electro-) chemical reduction. A: During potential-controlled electrodeposition additionally to the current conduction a second wire connection is often established to the working electrode (WE) to enable a separate detection of the electrode potential (four point measurement) against a reference electrode (REF). B: During electroless deposition, no counter electrode (CE) is required. An optional measurement of the electrode potential against a reference electrode can be used for process monitoring. C: No wire connections are required or applicable in case of nanoparticle synthesis.

the *electroactive species* and hence slow down the deposition rate. The role of the ligand is discussed elsewhere in more detail.^[65]

Along with step 3 an adsorption of the platinum ion at the surface of the electrode (*adion*) and a final integration of the *adion* into the electrode structure proceeds. According to thermodynamics the deposited platinum *adion* has to travel via surface diffusion to a kink site for final reduction and integration into the structure of the electrode (*crystal growth*) in order to minimize the surface energy of the solid.^[73] *Crystal growth* will lead to a smooth surface. To generate a porous deposit the formation of new clusters of deposited adions (*nucleation*) has to occur at a high rate. According to thermodynamics the generation of such new clusters at the electrode surface is disabled due to an increase in surface energy. This is different once a critical cluster size is reached and the free energy gain related to cluster growth (energy gain according to phase transition) is able to balance the increase in surface energy. For cluster sizes larger than this critical size the free energy gain overbalances the surface energy losses and a further growth of these nuclei is thermodynamically supported according to classical nucleation theory.^[74–76] In other words an activation energy barrier has to be overcome to form nuclei of stable size and thus surfaces of a porous nature. The number of molecules N_c in a cluster of critical size can be expressed for a spherical 3D-nucleus by:

$$N_c = \frac{32\pi v_m^2 \sigma^3}{3|\Delta\mu|^3} \quad (1)$$

Here σ , v_m and $\Delta\mu$ stand for the surface tension, volume per molecule and difference in electrochemical potential between the solvated and deposited state, respectively. During electrochemical deposition the difference in electrochemical potential can be regulated by the applied overpotential η ^[73] according to

$$\Delta\mu = zF\eta \quad (2)$$

Here z and F represent the number of transferred electrons per ion and the Faraday constant, respectively. Accordingly, high

overpotentials (relative to the reversible deposition potential) can be used to decrease the critical cluster size and thus to facilitate *nucleation*. This way *nucleation rate* is enhanced compared to crystal growth rate resulting in a more porous structure.

Porous structures in particular develop if the deposition current density j_{dep} is chosen close to the *limiting current density* j_{lim} of the system.^[73] The *limiting current density* characterizes the maximum rate of mass transfer of the *electroactive species* from the bulk to the electrode. Hence in the case of j_{dep} is in the range of j_{lim} or higher all of the *electroactive species* is deposited immediately as it reaches the electrode without further surface diffusion of the *adion* towards a low-energy position. Considering step 1 to be the limiting step in the supply of *electroactive species* the *limiting current density* is given by

$$j_{lim} = \frac{nFDc_{bulk}}{\delta_{Nernst}} \quad (3)$$

Here n stands for the number of transferred electrons per ion, F is the Faraday constant, D the diffusion constant, c_{bulk} the concentration of the complex ion in bulk solution and δ_{Nernst} the thickness of the Nernst diffusion layer.

Also surface defects (typically 10^8 defects per cm^2 in metals) play an important role during electrodeposition.^[73] This is because on the one hand they represent favored positions for *nucleation*. On the other hand protruding points or edges lead to a concentration of the electric field and hence to a locally enhanced deposition current. The effects on the character of the growing structure are summarized in **Figure 3**.

2.2. Chemical Reduction

In an *electrochemical reduction* the electrons are provided by the cathode (working electrode) and an external power source, respectively. In contrast to this, in a *chemical reduction* the electrons are transferred from an in parallel proceeding oxidation

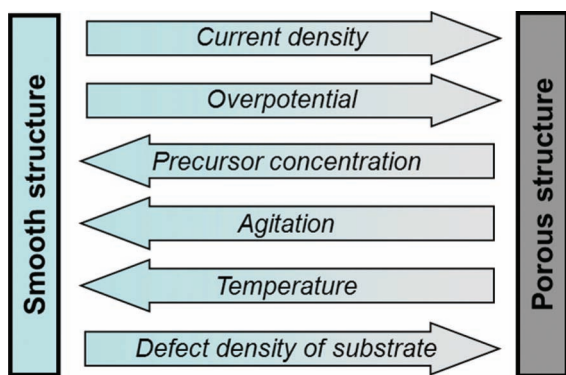


Figure 3. Strategies enabling the fabrication of porous platinum electrodes according to reference [73]. An increase in the parameter changes the character of the structure as indicated by the arrow (e.g., a higher current density leads to a more porous structure).

of a reducing agent. During this process the *reducing agent Red* is oxidized to its oxidized form *Ox*:



Typical *reducing agents* include hydrogen, hydrazine, sodium borohydrate, citrate, ascorbic acid and alcohols (in particular polyols such as ethylene glycole). *Chemical reduction* can either be performed at an electrode surface which is termed *electroless deposition* or in solution which equates to *nanoparticle synthesis*.

2.2.1. Electroless Deposition

The reduction of platinum precursor by *electroless deposition* proceeds in almost the same manner as in *electrochemical deposition*, with the difference that electrons are not provided by an external source but a reducing agent. Consequently the supply of the reducing agent can also represent the rate determining step. During deposition the whole electrode (working electrode) serves as catalyst which means a fast electron exchange between the site of *reducing agent* oxidation and platinum reduction occurs via the electrode as indicated in Figure 2B (*heterogeneous nucleation*).

For electroless deposition no wire connections are required in principle. Nevertheless a wire connection can be advantageous since changing open circuit potential of the electrode during the deposition process reflects the changing nature of the electrode and can thus be utilized for process monitoring.^[73]

In the context of porous platinum *electroless deposition* is applied for fabrication of *substrate-based* and in *decoration* methods. Also the combination of *electroless deposition* with templating techniques (see Section 4.3^[77]) is often found in literature.

2.2.2. Nanoparticle Synthesis

Platinum nanoparticles are synthesized by an autocatalytic chemical reduction of metal salt in aqueous or non-aqueous solution in presence of a reducing agent (see Figure 2C).^[61,62,75] During this *nanoparticle synthesis* the newly generated particle surfaces serve as catalyst for the further reduction of platinum ions (*homogeneous nucleation*). A typical setup for such a synthesis does not provide or require electrical connections.

Nevertheless process monitoring is possible since the particle formation induces a change in the colour of the solution. Hence even a quantitative process monitoring can be performed using UV-Vis spectroscopy.^[78–81]

In most cases nanoparticles are synthesized in solutions which consist of a solvent, platinum salt, reducing agent, stabilizer or capping agent and sometimes buffer salts to control the pH. Capping agents are organic or inorganic ligands that adsorb onto the surface of nanoparticles. The adsorption of such ligands and their steric demand prevents direct interconnection between neighboring particles and hence prevents small particles from agglomeration.^[63] Moreover the adsorption of capping agents depends on the specific surface orientation. Thus the choice and concentration can be used to control their microscopic shape (see Section 3.1.^[33]).

Besides synthesis in aqueous media, the polyol process represents a very common synthetic route. Here the polyol (ethylene glycole in most cases) acts as solvent as well as reducing agent.^[62,82–85] Since ethylene glycole is a weak reducing agent, the reduction process is comparably slow. Therefore just adsorbed adions have enough time during the reaction process to find a kink site in the crystal structure leading to narrow size and shape distributions. Heating of the solution to about 110 °C is required to activate nanoparticle synthesis in such a polyol process.^[83] In a process modification termed microwave-assisted polyol process this heating is achieved by interaction of the microwaves with electrical dipoles in solution.^[85–87] This way the solution volume can be heated without heating the walls and thus nucleation on the walls can be avoided, which is advantageous in industrial applications.^[86]

As during the electrochemical reduction process, nanoparticle formation proceeds in a sequence of nucleation and crystal growth. During nucleation a critical cluster size needs to be reached in order to thermodynamically enable further particle growth. Often nucleation is assumed to start if the concentration of zero-valent (already reduced) atoms reaches a certain superconcentration and clusters of zero-valent atoms form according to a mechanism proposed by LaMer.^[34,88] This is contradictory to publications by Henglein et al.^[78] and molecular dynamics simulations by Ciacchi et al.^[89] Both studies exclude a zero-valent intermediate from energetic considerations and reveal a Pt(I)-Pt(I) dimer as most probable first intermediate in the reduction of $[\text{PtCl}_2(\text{H}_2\text{O})_2]$ (predominant complex formed from H_2PtCl_4 in water). Moreover, the simulations of Ciacchi et al. showed a significantly higher electron affinity for the dimers and trimers compared to the complex-ion. So it can be concluded that in first stage a still charged Pt(I)-Pt(I) dimer is formed. This dimer is supposed to be coordinated and stabilized by chloride ions and grows by addition of further charged platinum ions. The charge is stabilized throughout the cluster and step by step reduced by electron transfer from the reducing agent.^[89] This way the cluster grows step by step leading to the formation of a stable nucleus.

This critical cluster size can be expressed for a colloidal particle according to classical nucleation theory by:

$$r_{\text{crit}} = \frac{2\gamma V_m}{RT \ln S} \quad (5)$$

Here γ stands for the surface free energy, V_m for the molar volume of the bulk crystal, R for the ideal gas constant, T for

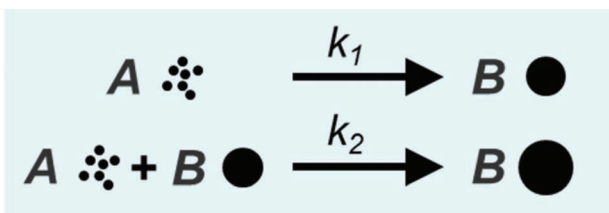


Figure 4. 2-step Finke-Watzky mechanism for the formation of transition-metal nanoparticles. In this kinetic model *A* represents the precursor and *B* the surface sites on the growing nanoparticles. Nucleation proceeds at a rate constant k_1 , and subsequent fast growth of the particle at a rate constant k_2 .

the absolute temperature and *S* for the degree of supersaturation (ratio of concentration to equilibrium saturation concentration). Further details on the description of the critical nucleation size can be found elsewhere.^[34,61,75] Comparable to the case of electrodeposition, particle growth is thermodynamically enabled when particle size exceeds this critical nucleus size.

As mentioned before, in case of nanoparticle synthesis particle growth occurs by an *autocatalytic growth mechanism* in which the nanoparticle's surface simultaneously functions as catalyst. Significant research has been performed on the understanding of the growth mechanism of such nano-clusters. A comprehensive review on mechanistic investigation of nanoparticle formation (*nucleation and growth*) has recently been published by Finney and Finke.^[75] Molecular dynamic simulations by Ciacchi et al.^[90] provided some insight into the growth process by showing that $\text{PtCl}_2(\text{H}_2\text{O})_2$ spontaneously adsorbs on Pt_{12} , $\text{Pt}_{12}\text{Cl}_4$ or $\text{Pt}_{13}\text{Cl}_6$ clusters without prior reduction. The electron transfer with the reducing agent is suggested to take place in a separate reaction involving the whole cluster. The derived growth mechanism for Pt-clusters is in agreement with the experimentally observed autocatalytic growth and shows in principle no difference to the nucleation mechanism. One approach for the kinetic description of nanoparticle formation is the 2-step Finke-Watzky mechanism which has successfully been applied to fit various kinetic data of nanoparticle growth.^[75,91] Here a slow *nucleation step* ($A \rightarrow B$) from precursor *A* and a subsequent fast *autocatalytic growth* ($A + B \rightarrow B$) on the surface sites of the nanoparticle (*B*) are assumed as indicated in the reaction schemes of **Figure 4**.

Based on this kinetic mechanism a ratio *R* of *growth to nucleation rate* can be defined and expressed by the rate constants for nucleation (k_1) and growth (k_2) as well as the concentration of surface sites on the growing nanoparticles c_B :

$$R = \frac{\text{growth rate}}{\text{nucleation rate}} = \frac{k_2 * c_{ACB}}{k_1 * c_A} = \frac{k_2}{k_1} c_B \quad (6)$$

This ratio *R* represents a measure to predict the character of the size distribution characteristic of the growing particles. At higher values of *R* particle growth is the predominant step and results in a homogeneous size distribution.^[91] Moreover, the diameter of the resulting nanoparticles also increases with *R*.

2.3 Further Reduction Pathways

Besides by electrochemical and chemical reduction with a reducing agent, platinum precursor reduction can be achieved by *photoreduction*, *radiolytic reduction*, *sonochemical reduction* or *thermal decomposition*.

Photoreduction of platinum complexes can either occur in a direct manner or via photosensitizing of the solvent or a photoactive additive.^[66,92,93] In a *direct photoreduction* process UV irradiation is absorbed by the platinum ion which initiates dissolution of the complex towards non-valent platinum by multi-step interactions with the solvent. *Photosensitizing* means that a photoactive reagent generates a reactive intermediate upon UV irradiation which reduces the precursor in a further step. In most cases radicals are formed as intermediate from alcoholic solvents or a photoactive additive such as porphyrin derivatives.^[66,81,92,94] The advantage of the *photosensitizing* strategy is a faster reaction kinetic and according to the free choice of photoactive reagent the excitation wavelength is not limited to the excitation range of platinum. Either way zero-valent atoms are expressed which form nuclei by coalescence similar to what has been described for nanoparticle formation in Section 2.2.2.

In *radiolytic synthesis* γ -radiation is used to create radicals in the solution acting as reducing agent for the reduction of the precursor, similar to in *photosensitizing*.^[66,95,96] Radicals are created in a homogeneous distribution with a high energy throughout the solution enabling the formation of small sized particles (~1 nm) and narrow size distributions.^[95]

In *sonochemical synthesis* high intensity ultrasound creates bubbles in solution which feature extreme conditions in terms of pressure (~1000 bar), temperature (~5000 K) and heating and cooling rates (~ 10^{10} K s^{-1}).^[67,97] Radicals form under these conditions from sonolysis of water, surfactants or other additives. A comparable nucleation and growth mechanism is expected as discussed for *radiolytic synthesis* since similar kinetics are observed.^[97]

Upon heating, platinum complexes undergo several *thermal decomposition* steps until finally a zero-valent metallic state is reached.^[98–100] This behaviour can be investigated by thermogravimetric analysis: For instance the aqueous complex $\text{H}_2\text{PtCl}_6 \cdot (\text{H}_2\text{O})_x$ gets completely dehydrated when reaching 170 °C. Subsequently H_2PtCl_6 is transformed stepwise into PtCl_4 , PtCl_2 and finally zero-valent Pt (>530 °C).^[99,100] For other precursors zero-valent platinum is observed already at lower temperatures: $(\text{NH}_4)_2\text{PtCl}_4$ (>330 °C), $(\text{NH}_3)_2\text{Pt}(\text{NO}_2)_2$ (>240 °C) or $\text{Pt}(\text{NH}_3)_4(\text{NO}_3)_2$ (>260 °C).^[100]

2.4 Structure Characterization

Typically, characterization experiments are performed to reveal elemental composition, particle sizes and specific surface area of the synthesized structures.

Elemental composition can be determined by well established techniques such as EDX (energy dispersive X-ray spectroscopy) and XPS (X-ray Photoelectron Spectroscopy).^[71,101] XPS has a smaller penetration depth compared to EDX and XPS-spectra provide information about the electronic states enabling further conclusions for instance about oxidation states. XRD techniques

(x-ray diffraction) enable conclusions on the present alloy phases.^[71,101,102] Moreover XRD results enable the calculation of average particle sizes on basis of the Scherrer equation,^[71,87,103] but in most cases particle size determination is performed via analysis of SEM (scanning electron microscopy) or TEM (transmission electron microscopy) images.^[71,101]

The surface area of platinum electrodes is usually determined electrochemically via charges related to hydrogen monolayer adsorption/desorption currents observed during cyclic voltammetry in sulfuric acid.^[104] CO-stripping and copper monolayer stripping represent alternative electrochemical methods.^[104–106] By comparison to the desorption or stripping charges to reference values known for a flat platinum surface an electrochemically active area can be determined. The *roughness factor* (RF) is a common representation for the surface roughness and is calculated as the ratio of the electrochemically active surface area to its projected footprint area. The *roughness factor* thus indicates the surface area enlargement resulting from the internal porous nature of an electrode. Alternative to electrochemical methods the surface area can be determined from gas adsorption isotherms in *BET-measurements* (called BET according to the initials of the original authors).^[107] According results are usually termed *BET-surface* and are presented in dimensions of surface area per mass ($\text{m}^2 \text{g}^{-1}$). Moreover to surface area measurement gas adsorption isotherms can be utilized to determine the pore size distribution.^[108] To analyze nanoparticle powder samples such as resulting from synthesis usually BET-analysis is chosen since no wire connections are required. In case of solid electrode structures, surface area determination is predominantly performed by electrochemical means, since BET-equipment is usually not designed for bulky samples.

3. Fabrication of Nanoparticle Based Platinum Electrodes

The extreme popularity of nanoparticles in catalysis within the last decade originates from several advantages over their corresponding bulk materials: According to their small size nanoparticles offer a high surface to volume ratio and thus promise a high degree of platinum utilization. The high flexibility in nanoparticle synthesis enables researchers to tailor catalysts at the length scale at which catalysis takes place. Moreover nanoparticles sometimes show catalytic effects (selectivity, activity) not known for the bulk material.^[6,109]

But sole nanoparticles do not yet constitute an electrode. At least an electrode has to be an electrically conductive compound structure connected to a current collector. With increasing current densities electrode performance will not only depend on the activity of the catalyst but also on the resistances for electric, ionic and mass transport. Only catalyst sites accessible to all these three transport processes can contribute to the electrochemical reaction. Therefore the introduction of an ion conducting component into the electrode structure and its pore architecture are key points in designing nanoparticle based electrodes.

In the following Section we will first discuss the basic techniques used in nanoparticle synthesis (Section 3.1) as well as modifications of these basic techniques (Section 3.2).

Subsequently, we introduce physical and chemical methods to immobilize nanoparticles onto a support material (Section 3.3). Finally strategies are discussed enabling the formation of a contiguous electrode structure from nanoparticles (Section 3.4).

3.1. Solution-Based Synthesis of Platinum Nanoparticles

Solution based colloidal synthesis is based on the reduction of a *platinum precursor* with a *reducing agent* in solution as discussed in Section 2.2.2. After a nucleus has formed an autocatalytic growth starts using the surface of the growing nanoparticle as catalyst. In the following we discuss several strategies to modify this basic principle in order to tailor nanoparticles in terms of size and shape.

All principles discussed for monometallic nanoparticles are in general also valid for the synthesis of alloyed nanoparticles. In this case a second metal precursor is added to the solution. This precursor simultaneously gets reduced with the platinum precursor during synthesis. Nanoparticle synthesis of all kinds of binary platinum alloys can be found in literature such as PtPd,^[110,111,112] PtAu,^[35,113–116] PtRu,^[35,87] PtFe,^[117,118] PtCu^[119] and others.^[33,40,61] The formation of mixed bimetallic phases in such nanoparticles and thus of truly alloyed nanoparticles is in most cases favored over the formation of separate monometallic phases due to an increase in entropy.^[61,116]

3.1.1. Size Control

Size control is crucial since the percentage of surface atoms and thus platinum utilization decreases with particle diameter.^[34,120] Moreover to platinum utilization, also the catalytic activity per surface area depends on particles size. Investigations performed with nanoparticles of only a few nm and sub-nm diameters have shown a decreasing specific catalytic activity with decreasing diameters.^[121–124] Maximum catalytic activities are typically obtained for diameters in the range of 2–5 nm.^[121,122]

Typical means to influence the particle size during synthesis include the choice of temperature, precursor concentration, reducing agent and capping agent as well as capping agent concentration. The particle size decreases with increasing nucleation rate in relation to the crystal growth rate and thus with decreasing critical nuclei size as discussed in Section 2.2.2 (see equation (5),(6)). Therefore high nucleation rates enabled by higher temperatures and high initial concentrations (degree of saturation) lead to a smaller particle size.^[61] Also strong reducing agents such as sodium borohydride or hydrazine facilitate the reduction of the precursor and hence promote nucleation in contrast to milder reducing agents such as sodium citrate.^[33,62] Since capping agents adsorb at the surface of the growing particle the growth rate decreases with increasing concentration of the capping agent, also leading to a lower particle size.^[61,78,125]

3.1.2. Size Distribution Control

Moreover to controlling the size of the synthesized nanoparticles a high uniformity in size distribution of the product is highly desired to control catalytic activity. For this it is critical

that all nuclei are formed at the same time and simultaneously develop through the different growth stages.^[61,62] In this case nanoparticles can grow to equal sizes. This can be achieved by a so called “burst nucleation” at high degrees of supersaturation (compare equation (5)). This way many nuclei form within a short time leading to a strong depletion in the degree of supersaturation and hence to an inhibition of further nucleation. Alternatively, a short and defined nucleation time can be realized by e.g. *photochemical activation*.^[81,92,93] Here, the nucleation time can be limited by the irradiation time and the *photocatalyst* concentration can be used to control the number of nuclei.

To obtain monodisperse particle sizes, growth should be stopped when precursor concentration diminishes, otherwise *Ostwald-ripening* occurs leading to a defocusing in size distribution.^[63] *Ostwald-ripening* describes the phenomenon that slightly larger particles grow by consumption of their slightly smaller neighbors. This phenomenon occurs according to equation (5): the diminishing precursor concentration leads to a significant increase in the critical nuclei size.^[63] Once *Ostwald-ripening* occurs during growth, the size distribution starts to split leading to a bimodal size distribution.

To prevent the occurrence of *Ostwald-ripening* capping agents are used in general. Alternatively, the process can be stopped before *Ostwald-ripening* starts. The resulting small particles can subsequently be transferred as seeds into a separate growth solution (*seed-growth process*).^[63] Since precursor reduction at seed surfaces (*heterogeneous growth*) is preferred over nucleation in solution (*homogeneous nucleation*) an epitaxial overgrowth of the seeds is obtained.^[33,61] For particle growth on the preformed seeds mild reducing agents and low temperatures are sufficient and can help suppressing any further nucleation. Hence *seed-growth* enables a separation of nucleation and growth phase and thus represents a method for control of size and shape.^[62] For instance, this way Han and co-workers observed an increasing dominance of hexapod shape and a more homogeneous size distribution in their synthesis for increasing concentration ratios of seed to precursor.^[126]

3.1.3. Shape Control

Another goal in nanoparticle synthesis is to control the microscopic shape and thus the predominant crystallographic surface orientation.^[3,31,127–129] The different crystal planes correspond to different geometrical arrangements of the surface platinum atoms and thus show different catalytic properties. Besides higher catalytic activity also reaction selectivity has been shown for some reactions such as aromatization or hydrogenation when using shape-controlled nanoparticles of only a single surface orientation.^[130–132]

In absence of interatomic interactions, a sphere represents the lowest energy state, since a sphere has the lowest surface area per volume and thus lowest interfacial energy. With growing number of shells electronic orbital interactions between neighboring atoms gain increasing influence on the energy state of the nanoparticle and lead to a rearrangement of the lattice according to geometric and energetic constraints of the atomic orbital structure. As a consequence of the directed orbital interactions, platinum crystallizes in a face-centered cubic lattice.^[62] Moreover each crystallographic orientation shows a different

surface energy: For low-index planes of platinum the surface energy increases slightly from (111) to (100) and more significantly to (110).^[33,61] Therefore, the thermodynamic equilibrium geometry of a platinum nanoparticle is a truncated octahedron, representing an energetic balance between increasing orbital interactions and an increasing surface area (see Figure 5A).

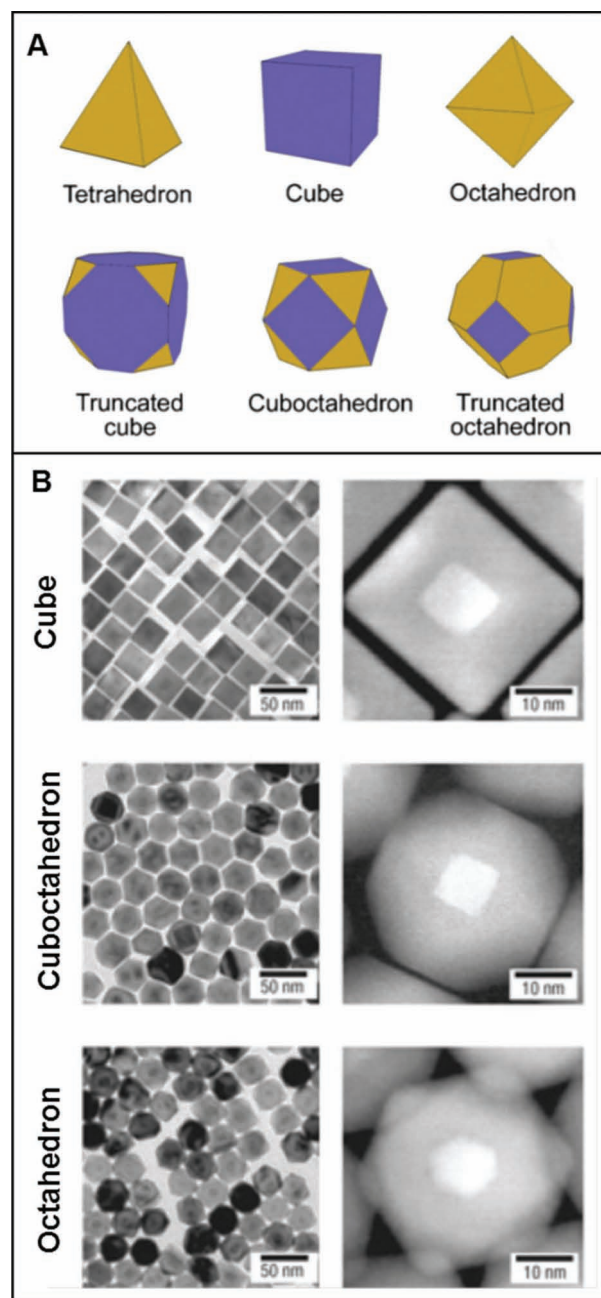


Figure 5. Shape controlled synthesis of nanoparticles. A: Overview about typical geometries. Crystal geometries in upper row feature only surfaces of one crystallographic orientation, geometries in lower row feature surfaces of two different orientations. Reproduced with permission.^[61] Copyright 2009, Elsevier. B: TEM (left) and high angle annular dark-field STEM (right) images of platinum nanoparticles synthesized in cubical, cuboctahedral and octahedral shape. Reproduced with permission.^[62]

A huge variety of different particle geometries have been synthesized with platinum today such as cubic, cuboctahedral or octahedral (see Figure 5,^[33,34,61,62]). Key to controlling the shape is to selectively control the growth kinetics along the different crystallographic orientations. Most prominent means for selective growth control is the choice and concentration of the capping agent which show specific adsorption properties on the different crystallographic planes. In one of the first works El-Sayed and coworkers synthesized nanoparticles with dominance of cubic and tetrahedral shape depending on the chosen concentration ratio between capping agent and precursor.^[125,133] Since then, various organic capping agents such as PVP (polyvinylpyrrolidone), citrate ions and various organic ammonium salts have successfully been applied to grow specific shapes.^[33,61,62] For instance PVP is known to preferentially bind to (111) and (100) planes. Therefore PVP can be utilized to protect these planes from further growth and thus enable to selectively grow crystals bound by (111) and (100)-planes. Moreover to organic capping agents, inorganic additives such as NO₂ or Ag⁺ can specifically adsorb to platinum surfaces and help controlling growth kinetics (decelerate or accelerate!).^[61,83]

3.2. Modifications to Solution Based Synthesis

3.2.1. Epitaxial Overgrowth for the Formation of Core-Shell Nanoparticles

Seed-growth has been described in Section 3.1.2 as a method for separation of nucleation and growth, but can also be used to fabricate bimetallic *core-shell* structures by epitaxial overgrowth with a second shell-metal.^[33,61] *Core-shell* nanoparticles (core @ shell) have been synthesized with all kinds of elements relevant to electrocatalysis such as for instance Pd@Pt, PtPd@Pt,^[134] Au@Pt,^[135–137] Ru@Pt,^[138,139] Ag@Pt^[140] as well as their counterparts Pt@Au^[135] and Pt@Ru.^[138] The *core-shell* approach can also be combined with fabrication of shaped nanoparticles. Here, Habas and co-workers observed an epitaxial overgrowth of palladium on cubic platinum seeds.^[141]

3.2.2. Synthesis of Hollow Platinum Nanoparticles

Hollow nanoparticles feature an inner cavity surrounded by a solid shell. Consequently, hollow nanoparticles have a lower density compared to solid nanoparticles due to their inner cavity and thus enable high catalytic activity at low platinum mass.^[44,110,142–145] Liu and co-workers applied hollow PtPd nanoparticles (on carbon nanotube substrate) to formic acid oxidation and demonstrated a five times higher catalytic activity compared to commercial fuel cell catalyst (E-TEK, PtRu at same catalyst loading).^[110]

In a conventional template based fabrication of *hollow nanoparticles*, platinum is deposited around functionalized spherical sacrificial templates such as polystyrene or silica spheres followed by template removal comparable to the methods shown in 3.2.3.^[94,144,146,147] Disadvantage of accordingly fabricated hollow structures is that they often suffer from an incomplete coverage and hence from a non-uniform shell thickness and structural fragility.^[145]

Alternatively, hollow platinum nanoparticles can be fabricated from less noble nanoparticles undergoing a *galvanic replacement reaction* (GRR, also see Section 4.4, 6.2) in a platinum precursor solution.^[143,148] According to the more positive redox-potential of platinum reduction compared to cobalt reduction, cobalt is dissolved in the presence of platinum ions. Consequently a platinum shell is deposited around a cobalt shell which further dissolves in the presence of platinum ions, finally leading to a hollow core. Platinum deposition preferentially occurs on the outer side because of the shorter diffusion pathway. The electrons for this reduction are transferred from the core-dissolution (cobalt oxidation) via the already deposited platinum structure.^[142] This way Liang and co-workers fabricated hollow nanoparticles of 24 ± 2 nm in diameter. The shell thickness of 2 nm was shown to consist out of 2 nm large nanoparticles. Following a similar synthetic process in presence of iodine Zheng and co-workers succeeded even in shape-selective fabrication of hollow nanocubes.^[149]

3.2.3. Templated Synthesis

Templating is a prevalent strategy in nanoparticle fabrication. Templates can be utilized during synthesis to predefine size and in some cases also the macroscopic shape of the nanoparticle. After synthesis the template has to be removed in order to extract the desired nanoparticles. Besides *soft templates* such as *liquid crystals* or *microemulsions* and *hard templates* such as *macroporous silica* also dendrimer molecules are today frequently used as a template at molecular scale.

Liquid crystals are formed by surfactant molecules if solved in water and *microemulsions* if surfactant molecules are solved in water-oil mixtures. Both systems can be used as template to direct particle growth and define structure geometries (see Figure 6).^[150–154] Different to in shape-control (Section 3.1.3) this control is limited to geometrical shape of the structure (e.g. tubes or spheres) and does not enable for definition of

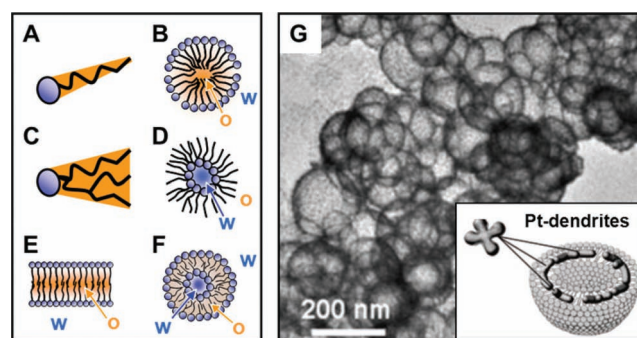


Figure 6. A–F: Building blocks of soft templating, with water and hydrophobic (or oil) phases indicated by “w” and “o”, respectively (prepared in the style of reference^[154]): Molecules with comparably large hydrophilic head (blue circle) as shown in A lead to micelle (see B) or cylindrical arrangements (see E) bringing their hydrophobic ends together (liquid crystal or oil in water emulsion). Surfactant molecules featuring a hydrophobic end with high steric requirement (C) prefer to form reverse micelles (water in oil microemulsion) as shown in D. F shows a liposome bilayer template. G shows an SEM-image of hollow platinum nanogages formed from Pt-dendrites grown in a liposome bilayer template (see inset). Reproduced with permission.^[156]

crystallographic surface orientations.^[154] In case of electrocatalytic application a complete surfactant removal is of particular importance in order to not affect the later catalytic activity.^[106,155]

Typical surfactants used for liquid crystal templating are Brij 76 (octaethyleneglycole monohexadecyl ether) as well as Tween 60 (sorbitan monostearate) or derivatives thereof. For instance Kijima and co-workers used mixtures of nonaethylene glycole monododecylether and Tween 60 in an aqueous solution of H_2PtCl_6 , nanotubes of 7 nm outer diameter and 2 nm wall thickness have been synthesized after reduction with hydrazine.^[153] The hollow structure of these tubes is a result of the hydrophobic core of the liquid crystal template. Song and co-workers reduced platinum in the presence of spherical liposome bilayer templates (see Figure 6F) and obtained hollow nanocages as shown in Figure 6G.^[92,156]

Different to in *liquid crystals*, consisting of either water and surfactant or oil and surfactant, *microemulsions* consist of water, oil and surfactant. For instance in water in oil *microemulsions* the inner water droplet represents a microreactor in which nanoparticles can be synthesized. The water content of the emulsion can be used to tune inner diameter of the resulting reverse micelles and hence enables control over the resulting particle size.^[154] For instance, using SDS (sodiumdodecylsulfate) as surfactant and pentanol/cyclohexane as co-surfactant Surendran and co-workers were able to fabricate cylinders with a tunable diameter (3 - 30 nm).^[157]

Mesoporous silica having a surface area of up to $1000 \text{ m}^2 \text{ g}^{-1}$ and typically pore sizes of 2–10 nm, can be used as *hard template* to predefine the diameter of the growing particles.^[2,158,159] Fukuoka and co-workers fabricated platinum nanoparticles of $2.4 \pm 0.2 \text{ nm}$ diameter by photoreduction inside of the pores of a hexagonal mesoporous silica (HMM-2).^[160,161] To isolate the nanoparticles from the non-conducting silica template, samples

were immersed in 1.5% HF and stabilized by triphenylphosphine (capping agent). The requirement for strong chemicals such as HF to remove the template after synthesis represents a significant disadvantage compared to *soft templating techniques*. Also without template removal such decorated silica find various applications in non-electrochemical catalysis.^[2]

Dendrimers are repeatedly branched molecules. Stable nanoparticle clusters can be synthesized by mixing platinum precursor with a *dendrimer* molecule, leading to a complexation of the precursor with functional groups of the *dendrimer* inside the branched molecule.^[123,124,162] Finally, precursor is reduced with a reducing agent leading to platinum clusters of monodisperse diameter predefined by the molecular geometry of the *dendrimer*. Particle size of the resulting clusters can be controlled by the type of dendrimer and its stoichiometric ratio to the precursor. By variation of the stoichiometric ratio Yamamoto and co-workers synthesized platinum clusters of only 12, 28 and 60 atoms, respectively (see Figure 7^[123]).

3.2.4. Further Strategies for Nanoparticle Synthesis

In several publications on nanoparticle synthesis precursor and reducing agent are distributed into two different immiscible liquid phases. Consequently nanoparticle synthesis occurs spatially limited to the *liquid-liquid-interface*.^[163–166] This way Rao and coworkers even observed the formation of contiguous nanoparticle networks (^[167], also see Section 3.4.2).

The reduction of platinum precursors by ultrasound induced radicals (*sonochemical* synthesis, compare Section 2.3) is another technology that can be found in literature on nanoparticle synthesis.^[147,168,169] Moreover to this, ultrasound can be used for nanoparticle synthesis in combination with *electrodeposition* in so-called *sonoelectrochemical* techniques. Here, an electric current pulse leads to nucleation of platinum particles at the

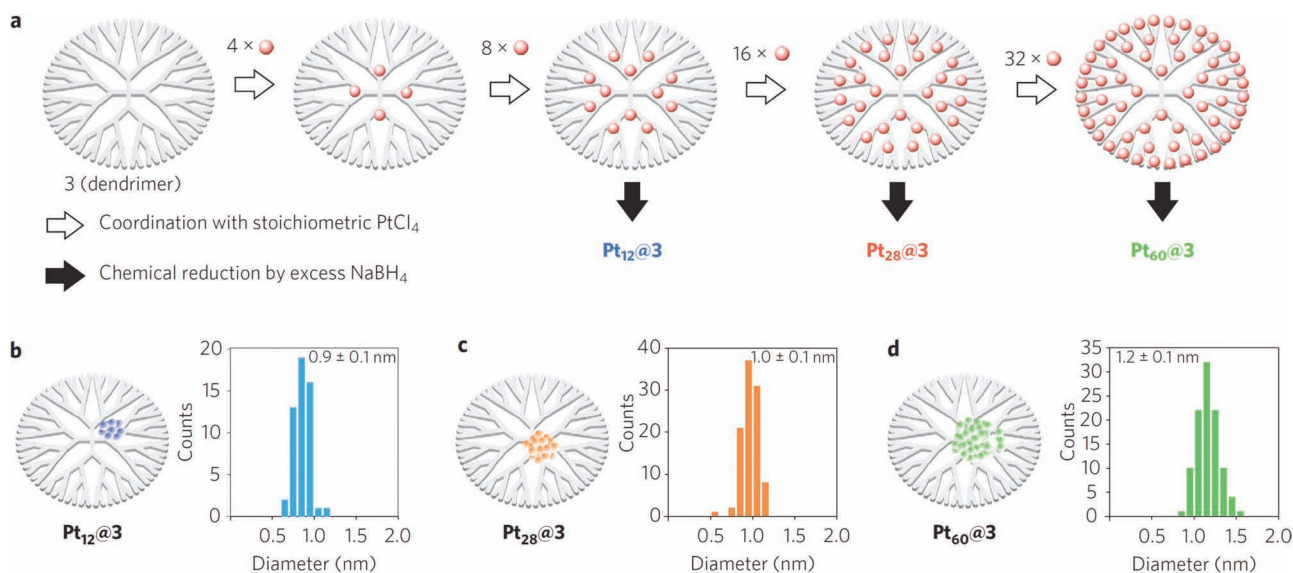


Figure 7. Schematic representation of dendrimer templated synthesis. A: Complexation of platinum metal ions in dependence of stoichiometric ratio to dendrimer molecules. B–D: Representation of the clusters formed by reduction with NaBH_4 in the specific stoichiometry indicated in A and the corresponding experimentally obtained particle size distributions. Reprinted with permission.^[123] Copyright 2009, Macmillan Publishers Ltd: Nature Chemistry.

electrode surface which are subsequently removed from the cathode by an ultrasonic pulse.^[170,171]

Electrospraying technology has been demonstrated in nanoparticle synthesis in two different ways: First approach is to dispense the precursor solution as aerosol into a solution containing reducing and capping agent.^[172,173] Second approach is to spray the precursor aerosol onto a heated substrate followed by *thermal decomposition* (above 500 °C in case of H₂PtCl₆^[174]).^[1,174]

Laser ablation represents a physical method to nanoparticle synthesis.^[66,175–180] Here, a pulsed laser is focused on a platinum metal plate immersed in solution, resulting in heating and ionization leading to the excavation of individual platinum atoms. By collisions these atoms grow to nanoparticles. Using laser ablation about 1 mg of nanoparticles can be prepared within 100 s. The use of capping agents is not mandatory in this method.

3.3. Fabrication of Supported Nanoparticles

An additional step is often applied into the electrode fabrication process in which the platinum nanoparticles get finely dispersed over a high surface area support material such as carbon black, carbon nanotubes (CNT) or similar (see 3.4.1 for further comments on the choice of support materials). The application of catalyst support materials enables a high platinum utilization due to a high dispersion of the catalytic platinum nanoparticles. This way significantly lower platinum loadings are required compared to in non-supported platinum-black electrodes.^[40,68,181] Hence the introduction of low-cost support materials into the fabrication process can lead to cost reductions of more than one order of magnitude.^[10]

3.3.1. Adsorption Based Decoration of Catalyst Support Materials by Nanoparticles

A decoration of catalyst support materials can be achieved by physical adsorption of previously synthesized nanoparticles on the surface of the support material.^[181] For this purpose, the support material is added to the colloidal nanoparticle solution followed by intensive mixing.^[114] This way nanoparticle synthesis and connection to the support material proceed in two independent steps enabling the use of all discussed strategies available for solution-based nanoparticle synthesis.

3.3.2. Impregnation: Synthesis of Nanoparticles on Catalyst Support Materials

Alternatively, nanoparticles can be directly synthesized/ reduced on the surface of the support material which corresponds to a heterogeneous nucleation process.^[63,181] Since heterogeneous nucleation is always thermodynamically preferred over homogeneous nucleation in solution, nanoparticle formation will predominantly occur on the surface of the support material and not within the volume of the solution.^[61] Different to nanoparticle growth in solution which is characterized by a spherically symmetric deposition process, heterogeneous nucleation and growth process is predominantly controlled by geometry of and

electronic interactions with the support material. Nevertheless, similar approaches as in solution based synthesis can be used for size control in impregnation.^[82,182]

In a typical protocol of a polyol impregnation process Lin and co-workers suspended carbon nanotubes (CNT) and sodium dodecylsulfate (SDS, surfactant) in ethylene glycole (EG, solvent and reducing agent).^[82] After ultrasonication of the mixture the platinum precursor is added and the solution is heated to an appropriate reaction temperature (140 °C). Their nanoparticles showed a large contact area to the nanotubes as consequence of the heterogeneous nucleation on the CNT surface and thus a limited symmetry (see **Figure 8**). This way they achieved a uniform dispersion of platinum nanoparticles without prior creation of nucleation sites by surface functionalization treatment. This is important since functionalization breaks the symmetry of the nanotubes π -bonding system and thus reduces electric conductivity. In a similar way impregnation of CNTs and graphene nanosheets were implemented using microwave-assisted polyol processes.^[183,184]

A further approach to impregnate CNTs has recently been shown by Ryu and co-workers, in which they generated platinum islands (about 100 nm in diameter) on CNT-mats by sputtering followed by an *intense pulsed light treatment*.^[185] Island formation is explained according to surface-energy minimization. The surface energy of platinum surfaces is much higher than that of CNTs.

In another route Joo and co-workers formed an ordered carbon powder from pyrolysis of SBA-15 (ordered mesoporous silica material) and subsequently impregnated it in an acetone solution of H₂PtCl₆.^[186] After impregnation they reduced the platinum in a hydrogen stream at 300 °C.

3.4. Electrode Formation from Nanoparticles

3.4.1. Binder-Assisted Electrode Formation

In sensor research or for electrochemical characterization of novel materials, a very simple protocol is often sufficient to

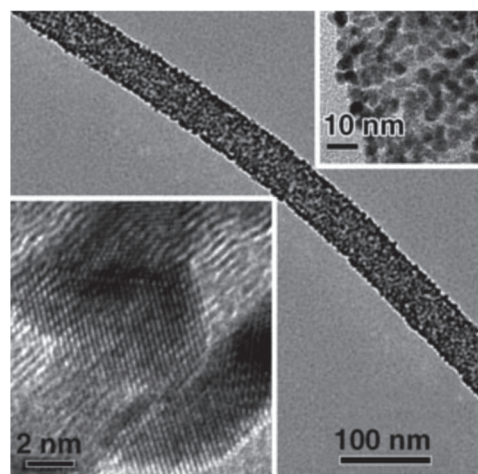


Figure 8. TEM images of platinum nanoparticles directly reduced on a multiwalled carbon nanotube. Reproduced with permission.^[82]

create an electrode: Colloidal solutions of supported or unsupported catalyst particles are dried on a glassy carbon electrode or other conductive substrate (current collector) and subsequently coated with a thin layer of Nafion for fixation purpose and ionic conductivity.^[187]

Reproducibility as well as homogeneity in density and height can be increased by using more automated deposition methods. For instance, *electrospraying* can be used to deposit preformed nanoparticles onto various substrates such as silicon, glass or titanium.^[173,188,189] While passing through the nozzle of an *electrospraying* device the liquid gets atomized to an aerosol by means of a strong electric field between the nozzle and the substrate. This way finely divided droplets containing only few nanoparticles can be deposited from a colloidal solution onto substrate surfaces forming nanostructured catalyst surfaces. Other techniques comprise screen printing, spraying, inkjet printing or casting.^[68,190]

To find an ideal balance between *electron, ion and mass transport* for the actual operation conditions represents the key task in electrode design for application in e.g. fuel cells or metal hydride batteries. Typically electrodes for polymer electrolyte membrane (PEM) fuel cells are composed of a current collector (usually the gas diffusion layer - GDL), membrane and the catalyst layer, as shown in **Figure 9**. In most cases the catalyst layer is fabricated according to a patent of Wilson and co-workers from 1993.^[191,192] This so-called *thin film fabrication technique* comprises three steps: ink preparation, ink deposition, and post deposition treatment.^[68] The ink usually consists of a mixture of catalyst particles, ionomer, water and an organic solvent to adjust the viscosity. To generate a homogenous layer, deposition is usually performed by either screen printing, spraying, or casting techniques.^[69,193] In particular screen printing and spraying represent well established methods that also allow for a reproducible fabrication of large scale electrodes. After

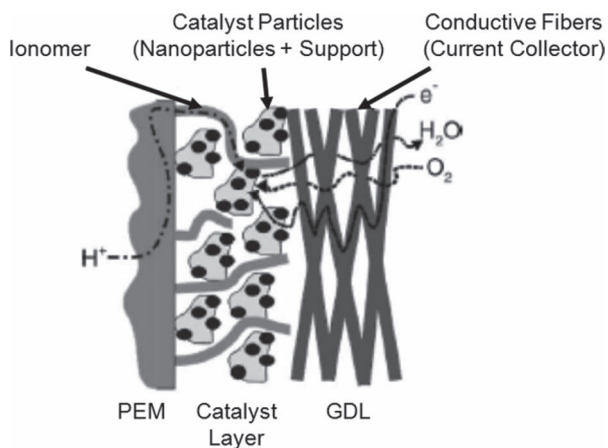


Figure 9. Schematic cross section of a typical structure of a polymer electrolyte membrane (PEM) fuel cell electrode fabricated from catalyst particles (nanoparticles on carbon support). The catalyst layer containing catalyst particles, ionomer and a pore system is pressed between them membrane (PEM) and the gas diffusion layer (GDL). Only sites on the catalyst particles with access to proton, mass and electron conduction (three-phase-boundary) can contribute to electrochemical activity of the electrode. Reproduced with permission.^[68] Copyright 2004 Elsevier.

deposition the ink is dried and sometimes hot pressing or similar techniques are applied to enhance cohesion of the catalyst layer to the membrane or gas diffusion layer.

Besides fabrication issues the choice of the support material represents another key feature in designing a high-performance electrode. For several years carbon black (Vulcan XC 72) has been the most popular material offering a high BET surface area of $230 \text{ m}^2 \text{ g}^{-1}$.^[194] Unfortunately a significant fraction of this surface area cannot be used, since it is situated within nanopores ($<2 \text{ nm}$) and thus it is hardly accessible to mass transport and no ionomer coverage can be established.^[194,195] Therefore a trend in research towards predominantly mesoporous and macroporous materials such as carbon aerogels,^[195] hollow carbon capsules,^[196,197] ordered hierarchical carbons^[198] and similar can be observed.

State of the art PEM fuel cell electrodes (based on carbon black) often suffer from incomplete electrical interconnection. About 70% of the catalyst particles are not connected to the current collector and thus cannot contribute to current generation.^[199] Therefore research in the field of support materials deals with materials enabling improved electrical connection pathways. E.g. carbon nanotubes are frequently used as support materials in current research articles. According to their longer length, they enable higher degree of electrical interconnection compared to carbon black.^[13,200] In a further approach carbon nanotubes were directly grown on the current collector to have a direct electrical connection between the current collector and the individual catalyst particles.^[199]

3.4.2. Binder-Less Fabrication of Platinum Nanoparticle Networks

Nanoparticle networks represent approaches aiming at the binderless bottom-up synthesis of porous platinum by physical or chemical interconnections between single nanoparticles.^[201] Driving force behind these bottom-up strategies is the wish to tailor 3D-architectures combining the strengths of size- and shape control known for nanoparticle synthesis with the ease of handling of macroscopic solids.^[202] The length scale that has been achieved for such networks ranges from 100 nm ^[202–205] to some mm ^[201] and even cm .^[206] Most publications on platinum networks are focused on the network synthesis only, but also the application to electrochemistry or surface enhanced raman spectroscopy have been reported.^[206,207] Linking strategies include physical interactions such as colloidal self-assembly,^[202,206,207] chemical crosslinking (such as di-thiols),^[201,204] synthesis at the liquid/liquid interface (^[167], see Section 3.2.4) and laser irradiation.^[203,208]

Yang and co-workers fabricated porous platinum froths with a high surface roughness (roughness factor = 1600) by reduction of H_2PtCl_6 with formic acid in absence of stabilization agents.^[207] CO_2 bubbles emerging from this reaction absorb at the forming nanoparticles and lift them up to the water-air interface by their buoyancy. Here platinum particles agglomerate to a froth film of about $10 \mu\text{m}$ thickness at the water-air interface (see **Figure 10**). From TEM observations the network structure was shown to consist out of primary particles of about 4 nm in diameter.

Park and co-workers used self-assembly of gold nanoparticles on a water-hexane interface to fabricate nanoparticle

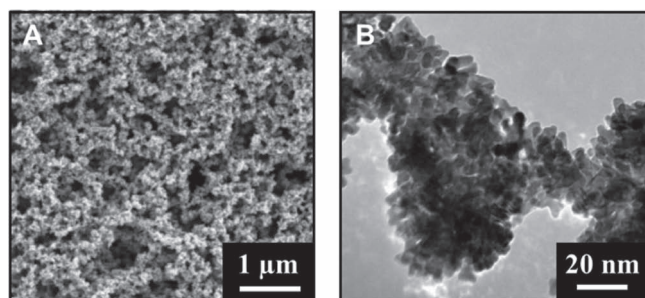


Figure 10. A: SEM image and B: TEM image of a platinum froth fabricated on water-air interface with the aid of buoyancy of CO₂ bubbles. Reprinted with permission.^[207] Copyright 2008, American Chemical Society.

networks.^[206] By lifting an ITO (indium tin oxide) substrate from underneath of the resulting densely packed film of gold nanoparticles they succeeded in transferring the film to the substrate. To create a catalytically active platinum surface they decorated the gold surface by underpotential deposition of copper followed by a galvanic replacement reaction (GRR) of copper in presence of platinum ions (for further details on the decoration procedure see Section 6.2).

Ramanth and co-workers showed a different approach based on the addition of toluene (drop by drop) to an aqueous colloidal gold suspension.^[202] Since toluene is able to replace the previous adsorbants (mostly anions) on the gold nanoparticles, toluene covered particles start to move upwards in water towards the water-toluene interphase. Moreover the replacement of charged anionic ligands by neutral toluene leads to a reduced electrostatic repulsion between the individual nanoparticles and thus promotes agglomeration. Consequently a film formation is observed at the interface.

Klajn and co-workers succeeded in fabricating nanoporous metals based on di-thiol interconnections.^[201] Thiol-groups are known to form strong bonds to noble metal surfaces and thus di-thiols can be used to interconnect individual nanoparticles. Consequently after addition of di-octanedithiol to a solution of individual nanoparticles (5.5 nm diameter), individual nanoparticles were observed to interconnect and to form supraspheres of 80–320 nm in diameter. After heating the supraspheres in toluene to 110 °C, a further agglomeration was observed leading to the formation of nanoporous metals of mm-size. In general, the use of interconnecting molecules to connect individual nanoparticles has a significant drawback, since such molecules negatively affect the catalytic activity of the nanoparticles.^[204,206] In the here discussed thiol based method this problem is solved during the heating step since thiols are known to desorb above 95 °C. Accordingly Klajn and coworkers found no residues of the interconnecting molecules in these structures by EDX and XPS. Once the supraspheres are brought in contact by the interconnecting molecules they stick together, even when the interconnecting molecules are removed.

Instead of di-thiols, Xie and co-workers used an addition of carbon monoxide during precursor reduction to synthesize platinum networks of 200 nm length from 2 nm platinum nanoparticles.^[204] The same behaviour was observed in case of carbon monoxide addition after reduction. In both cases, the presence of CO leads to the formation of so-called Chini-clusters

([Pt₃(CO)₆]_n²⁻) at the surface of the nanoparticles. Since platinum atoms within Chini-clusters have a strong affinity to form Pt-Pt bonds, particle interconnection is obtained as a self-organization process.

3.5. Discussion

Nanoparticle synthesis offers the opportunity to tailor the catalyst in terms of elemental composition, size, morphology and exposed crystallographic planes. At a small particle size nearly all platinum atoms contribute to the catalytic activity, accordingly fabricated electrodes thus profit from high platinum utilization. These designing opportunities were shown to enable a significant enhancement in catalysts in terms of catalytic activity and product or reaction selectivity. High catalytic activity has been demonstrated in electrochemical applications but until today reaction selectivity has only been proved in chemical catalysis. The most developed synthetic approach is solution based precursor reduction by a reducing agent in presence of stabilizing agents such as polymers or inorganic additives to control size and shape of the nanoparticles. Reduction approaches based on either photochemistry, sonochemistry, sonoelectrochemistry or thermal decomposition represent less common alternative strategies with specific strengths depending on the desired application.

Electrode formation from nanoparticles is usually achieved by deposition of an ink containing platinum nanoparticles on a carbon support material. The surface roughness can be varied by the thickness of the catalyst layer. The complete removal of surfactant molecules from the nanoparticles as well as their dispersion on the support is of great importance for their catalytic activity.^[106] The structural stability of nanoparticles is still a critical issue limiting the long-term stability of such electrodes and thus represents a key challenge in future. Nanoparticle networks represent an alternative electrode formation approach to form free-standing porous platinum. Today the applicability is still limited due to small size and fragility.

4. Fabrication of Substrate-Based Platinum Electrodes

Within this Section we show top-down approaches to porous platinum electrodes using an already contiguous and conductive electrode as starting point. This electrode is refined to form a highly active electrocatalyst structure on top of it by means of electrodeposition (Section 4.1 and 4.2), electroless deposition (Section 4.3), galvanic replacement (Section 4.4), thermal decomposition (Section 4.5) or chemical vapor deposition (Section 4.6). According to its significance two Sections are dedicated to electrodeposition methods: Section 4.1 shows the different electrodeposition techniques and Section 4.2 their combination with soft, hard and colloidal templates.

4.1. Electrodeposition (template-free)

Fabrication of platinized platinum or platinum black electrodes by electrodeposition is as old as elegant approach ranging back

to the 19th century.^[209] Electrodeposition techniques take advantage of high controllability. Different to colloidal synthesis the process parameters as well as the process duration are controlled externally via a current source. Another characteristic is that the deposition is restricted to conductive areas enabling the fabrication of structured electrode arrays as for instance required in neural stimulation.^[22–24] Moreover the deposit is covalently bond to the substrate which functions as current collector enabling a stable structural network at low electrical resistivity.

The electrodeposition step itself can be performed either by galvanostatic, potentiostatic or by potentiocyclic methods.^[73,210] Galvanostatic depositions feature the advantage that the deposited charge can easily set by deposition time, but the potential is not fixed and thus the exact electrochemical processes can vary during deposition. The application of a fixed deposition potential during potentiostatic deposition enables control over the proceeding process. To have a constant potential the current is regulated and thus potentiostatic methods show no linear correlation between time and deposited charge and mass, respectively. Park and coworkers investigated the evolution of surface roughness in potentiostatic deposition.^[211] For instance they observed the roughness factor (RF) to linearly depend on the deposited charge for RF values up to 250. At higher surface roughness a deviation from the linearity is observed which they explain by a partial enclosure of the pore system and thus reduced accessibility of the internal surface resulting from extended platinum deposition. For more negative deposition potentials they observed a higher surface roughness and an increasing number of cracks on the fabricated surfaces.

Besides the standard potentiostatic and galvanostatic methods modifications thereof were introduced such as pulsed electrodeposition (see Section 4.1.4) and deposition during potential cycling.^[51,52,212–214] Pulsed electrodeposition enables to alternate different potentials and thus different processes. For instance pulsed electrodeposition can be used to switch between deposition and non-deposition periods to reduce concentration gradients appearing during deposition in vicinity to the electrode surface. Electrodeposition during potential cycling (cyclic voltammetry) has the advantage that information about the growing structure can be extracted from peak and curvature changes in the cyclic voltammogram.^[51,52]

Alloy-based electrodes can be fabricated by co-deposition what is basically an in parallel proceeding electrodeposition of two or more metals from their salts.^[73] Co-deposition has successfully been applied to many relevant binary systems such as Pt-Au,^[215,216] Pt-Ru^[28,212,217] and Pt-Cu.^[218,219] Such a co-deposition is possible for deposition potentials chosen more reducing than the redox-potential of both compounds. In general the composition of the deposit differs from the concentration ratio in solution since as well deposition kinetics and the resulting overpotential are different for the individual metal precursors. Not in all cases co-deposition leads to truly alloyed phases, but also two separate phases can result depending on the chosen deposition parameters such as the deposition potential.^[73] The presence of a truly alloyed phases can for instance be confirmed by XRD-measurements.^[28]

Typical roughness factors of electrodeposited platinum are in the range of 20–500 without the use of support materials and

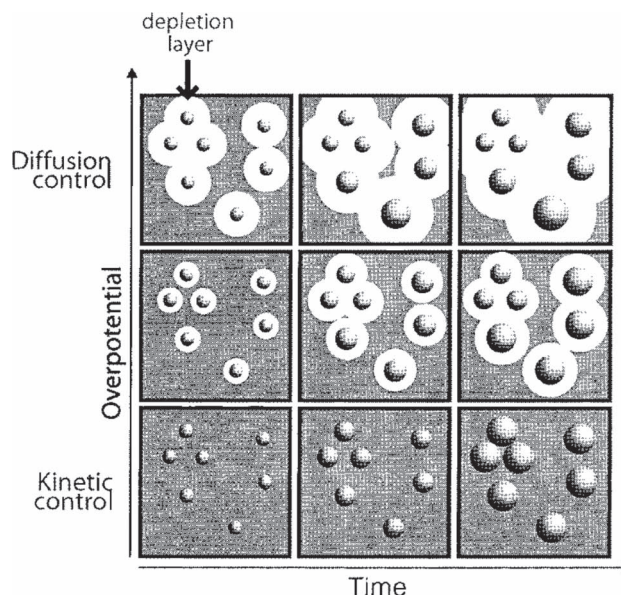


Figure 11. Illustration of the effect of overpotential and deposition time on the formation of *interparticle diffusion coupling* (IDC) during electrodeposition. Reprinted with permission.^[210] Copyright 2002, American Chemical Society.

up to 3000 for carbon supported systems.^[209,211] Roughness factors of up to higher than 3000 have been reported for electrode fabrication techniques combining electrodeposition and dealloying without the use of a high surface area support material (see Section 5.5).^[51,52,219]

4.1.1. Particle Size and Size Distribution Control

During electrodeposition nucleation sites are randomly distributed over the substrate surface resulting in an asymmetric overlapping of the diffusion fields of the individual nuclei (see Figure 11,^[210]). This effect is known as interparticle diffusion coupling (IDC). Consequently nuclei grow more slowly the higher the number and proximity of neighboring particles is.

One strategy to achieve a narrow size distribution is to apply reduced growth rates and hence to minimize the overlapping of the concentration depletion layers as shown in Figure 11. This is usually performed in a double pulse strategy consisting of a short nucleation pulse (high overpotential to create many nuclei, see Section 2.1) followed by the growth time at low overpotentials. This way size distributions with a coefficient of variation of as low as 7% have been reported for electrodeposition of platinum.^[220] Moreover, a reduction in particle size has been observed for such two step electrodeposits.^[221] In recent studies the addition of ethylene glycole (EG) to the electrolyte has been reported as an alternative method for narrowing the size distribution.^[222] Moreover Tsai and co-workers observed the presence of EG to reduce the average particle size of the electrodeposited Pt-Ru particles from 5.6 to 3.1 nm.^[222]

4.1.2. Shape Control

Only little research is published about template-free shape control in electrodeposition and the state of the art is not

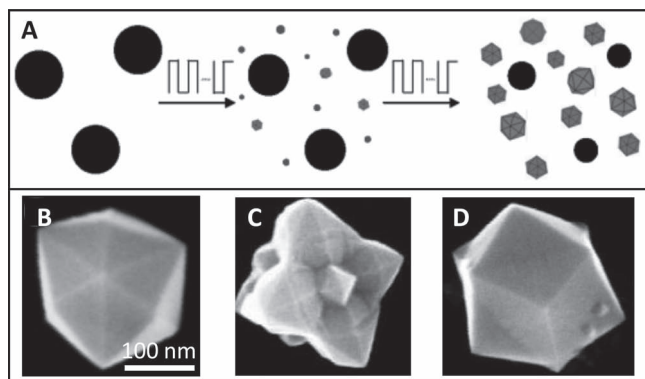


Figure 12. Electrochemical synthesis of high-index surface nanocrystals: A Schematic illustration of the fabrication process (see text for details). B–D show SEM images of tetrahedral nanocrystals bound by 24 (hk0) high-index facets (B), flowerlike nanocrystals consisting of several square pyramids bounded by (hk0) planes (C), concave hexoctahedral nanocrystals bound by 48 (hkl) high-index facets (D). Individual images are reprinted with permission.^[225] Copyright 2008, American Chemical Society.

comparable to what is known about shape control in solution based nanoparticle synthesis. Ye and co-workers observed a selective change in morphology of the deposit after addition of polyethylene glycol (PEG-10000) and lead acetate to the deposition electrolyte.^[223] Instead of spherical clusters, clump-like aggregates (100–200 nm in diameter) and flake-like structures (100–300 nm in length) were found using PEG-10000 and lead acetate, respectively.

In 2007 Tian and co-workers attracted a lot of attention with their two-step electrochemical synthesis of tetrahedral platinum single crystals.^[224] In a first step 750 nm large platinum nanospheres are deposited on glassy carbon by a double pulse technique from K_2PtCl_6 (see Figure 12A and supplementary information of ref. [224]). Subsequently a rearrangement of the platinum deposit is performed by a 10 Hz potentiostatic square wave treatment between -0.2 and 1.2 V versus SCE in a solution of 30 mmol l^{-1} ascorbic acid in 0.1 mol l^{-1} H_2SO_4 . They assumed the repetitive adsorption and desorption of oxygen enforced by the applied pulse scheme to play a key role in structure evolution. Besides tetrahedral, they succeeded in the synthesis of flowerlike and concave hexoctahedral shaped single crystals and multiple twinned nanorods (see Figure 12B–D). These shapes were achieved by elongation of the rearrangement step, replacement of ascorbic acid with citrate and air exposure after the first step, respectively.^[225] This way they showed the first electrochemical synthesis of platinum nanoparticles with strict crystallographic orientation. Although these publications on electrosynthesis of tetrahedral nanocrystals are highly cited in literature practical applications of such nanocrystals are still rare.^[226–228]

4.1.3. Electrodeposition onto Support Materials

Also in electrodeposition, high surface area supports such as carbon black,^[28,229] carbon nanotubes^[212,213,230,231] or boron doped diamond^[232] can be used to enable a high dispersion of platinum. Concerning the incorporation of ionomer into the electrode design two different process sequences exist: Either

the ionomer is coated to the electrode prior^[212,233,234] or past the electrodeposition step.^[28,229] The former process sequence has the advantage that platinum can only be deposited at the three phase boundary (presence of ionomer, pore volume and solid electrode structure, compare 3.4.1). The disadvantage of this process sequence is that chloride ions (a catalyst inhibitor^[235]) get enclosed within the electrode compound if chloroplatinum salts are used as precursor.^[229]

4.1.4. Pulsed Electrodeposition

The application of pulsed deposition using an alternation of deposition (on-time) and waiting time (off-time) has become a very popular modification to galvanostatic^[28,213,223,229] and potentiostatic deposition.^[215] During the waiting time a concentration relaxation and thus an in average higher concentration at the electrode surface is achieved compared to continuous deposition. The waiting time leads to a reduction of the depletion layer diameter (compare IDC in Figure 11). Accordingly higher current densities and thus higher overpotentials can be applied during the on-time enabling a finer crystal grain and higher surface area at equal deposition charges.^[229] Kim and co-workers investigated the influence of deposited charge, deposition current density and off-time on the active surface area and electrode polarization as PEM electrode and identified some limits of pulsed galvanostatic deposition. For instance, no increase in surface area is observed if the current density is chosen higher than 200 mA cm^{-2} . This can be explained by a strong hydrogen gas evolution caused by these high overpotentials which destroy fragile parts of the growing electrode structure. Moreover, the surface area was observed to show a maximum depending on the choice of duty cycles (ratio of on- to off-time). At too high duty cycles reactant supply is not sufficient limiting the deposition efficiency and thus surface growth. At too low duty cycles the precursor concentration is too high and thus the deposition current is significantly lower than limiting current, leading to a less dendritic structure growth. Similar effects are known for pulsed potentiostatic deposition.^[215]

4.2. Electrodeposition Through Templates

The use of sacrificial templates during electrodeposition represents a very powerful modification to pure electrodeposition. Such templates can either be of *hard* (e.g. solid membrane structure), *soft* (e.g. liquid-crystal) or *colloidal* (self-assembled microspheres) nature.^[158,236] As shown in Figure 13 templated electrodeposition can be used to grow substrate-bound platinum structures in various 3D structures such as for instance nanowires,^[18,19] nanobrushes, nanotubes^[17,237] or honeycomb networks.^[238,239]

4.2.1. Hard Templates

In *hard template* approaches platinum is electrodeposited inside the voids of a porous solid structure or membrane.^[158] For this purpose a conductive start-layer is established on the backside of a membrane template by either thermal evaporation, sputtering or deposition of nanoparticles.^[240] Starting from this conductive

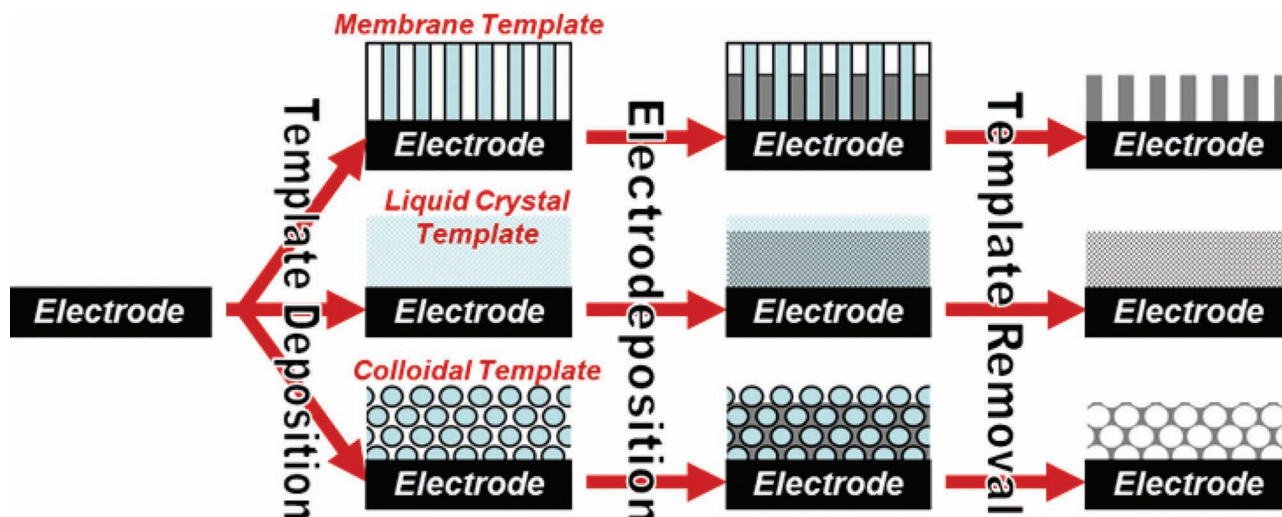


Figure 13. Schematic illustration of templated electrodeposition processes by using hard templates (e.g. membranes), soft templates (e.g. liquid crystals) or colloidal templates. The deposited platinum structures are indicated in dark grey.

layer platinum grows electrochemically along the pores of the template (see Figure 13). Finally the template is dissolved and free-standing nanowires are obtained which resemble the void structure of the membrane template. The length of the nanowires can be controlled by controlling the deposited charge during electrodeposition. To obtain nanotubes a preferential growth along the pore walls is prerequisite. For instance, this can be achieved by a pretreatment with molecular anchor molecules such as 3-aminopropyltrimethoxysilane (APTMS) or Se^{2+} -cations prior to platinum deposition.^[17,241,242]

Most prominent hard templates are anodized aluminium oxide membranes (AAO) and polycarbonate track etched (PC-TE) membranes, since they are commercially available and can easily be tuned in pore density and diameter.^[158,236] AAO membranes have regular order with pore diameters of 10 to 200 nm at pore densities of 10^9 to 10^{11} pores per cm^2 . The pores in PC-TE membranes are typically randomly distributed. Pore diameter can be chosen in the range of 10 nm to 10 μm and a pore density of up to 10^8 pores per cm^2 . Besides AAO and PC-TE membranes also silica membranes (see^[243] for a good overview) and few other materials are found in literature. For instance, Meldrum and Seshadri used the natural porosity of skeletal plates of sea-urchins as deposition template.^[244]

In a typical example for templated electrodeposition Yuan and co-workers fabricated arrays of hollow platinum nanotubes in anodized alumina membranes with a roughness factor of 760 (see Figure 14A).^[17] The obtained tubes had a length of 3 μm and inner and outer diameters of 70 nm and 150 nm, respectively. Predominant growth along the pore walls was achieved by a pretreatment of the membrane with 3-aminopropyltrimethoxysilane (APTMS).

Cui and co-workers also fabricated hollow platinum nanotubes through an anodized alumina membrane with a BET surface of about $12 \text{ m}^2 \text{ g}^{-1}$ using DMSO as solvent (see Figure 14B).^[245] They attributed the preferential growth along the pore walls to the use of DMSO as solvent. DMSO has a significantly higher viscosity compared to water, thus slowing down mass transfer to the bottom of the pores. Moreover the precursor PtCl_2 forms complex ions with high steric demand in DMSO ($\text{Pt}((\text{CH}_3)_2\text{SO})_2\text{Cl}_2$).

A double templating techniques was used by Park and co-workers to fabricate platinum-decorated gold nanotubes as shown in Figure 15.^[246,247] First they electrodeposited polyaniline (PANI) into the pores of an AAO membrane template. After drying at 80 $^\circ\text{C}$ the grown PANI was shrunk to pillars standing in the middle of the pores, leading to an overall template with tubular cavities which they filled with Au-Ag alloy by electrochemical co-deposition. By immersion in nitric acid they removed the two template materials and simultaneously dealloyed the Au-Ag nanotubes to porous Au nanotubes (see Section 5 for dealloying methods). The introduction of a dealloying

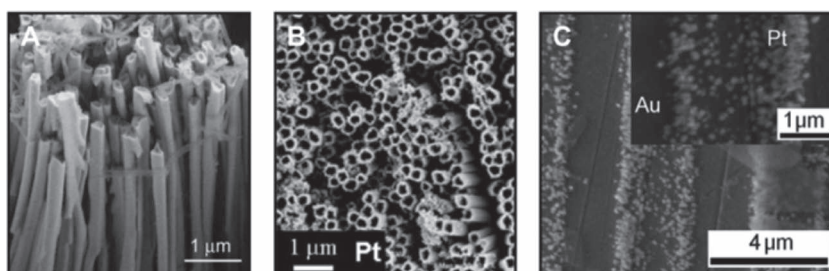


Figure 14. Hollow platinum nanotubes fabricated by electrodeposition in aqueous solution (A, Reproduced with permission.^[17]) and DMSO solution (B, Reproduced by permission.^[245] Copyright The Royal Society of Chemistry (RSC)) using anodized aluminium oxide membranes as templates. C: Platinum pattern on a gold substrate deposited through a lithographically patterned polyaniline film. Reprinted with permission.^[248] Copyright 2009, American Chemical Society.

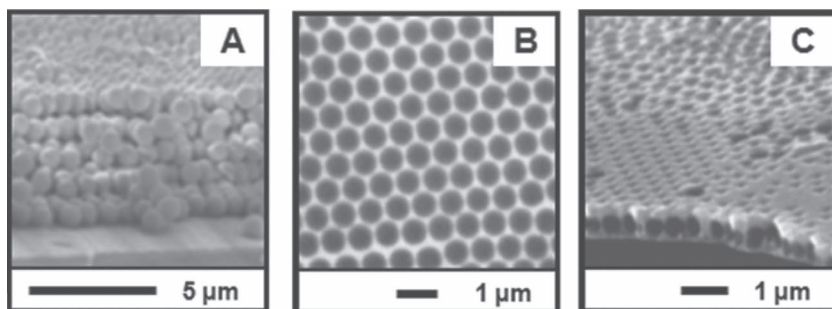


Figure 16. SEM images of a typical colloidal template made of polystyrene beads (A, Reproduced with permission.^[158] Copyright 2010 Springer) and structures resulting from electrodeposition into the template voids followed by template removal. B shows the structure from the top, C from the side. B,C are reprinted with permission.^[238] Copyright 2002 American Chemical Society.

by immersion of the sample into toluene and HF in case of polystyrene and silica microspheres, respectively. According to the wide diameter range of commercially available microspheres (100 nm to 250 μm) this technique allows for flexible design in pore and feature size. Song and co-workers used silica microspheres to form mesoporous electrodes for a glucose sensor.^[16] After potentiostatic deposition (0.05 V vs. SCE) of 0.8 C on a sample of 0.2 cm² they obtained mechanically stable films showing a roughness factors of 65 and 33 when using microspheres of 200 nm and 500 nm in diameter, respectively.

4.3. Electroless Deposition

The fabrication of substrate-based electrodes by electroless deposition can either start on flat as well as on already porous substrates such as highly ordered pyrolytic graphite. In case of already porous substrates, immersion of the substrate in the precursor solution period is usually applied before addition of the reducing agent to allow the precursor to get soaked into the pores. This way nanoparticles can form on the substrate surface in the same manner as described in impregnation approaches for nanoparticle synthesis in Section 3.3.2.^[71,198,255]

Starting from flat fluorine-doped tin oxide (FTO) Ouyang and co-workers fabricated strongly adhesive counter electrodes for dye-sensitized solar cells by a *polyol reduction process*.^[55,58] In a first step they coated an ethanol solution of H₂PtCl₆ onto a 1.9 × 1.9 cm² FTO substrate. After solvent evaporation the H₂PtCl₆ film was dried at 80 °C and covered with ethylene glycole. Subsequent heating to 160 °C for 15 min resulted in metallic platinum.

Hydrothermal synthesis represents an alternative electroless deposition technique which uses elevated temperature and pressure in a closed reactor.^[71] This way, Chen and co-workers utilized electroless deposition of platinum as well as Pt-Ru and Pt-Pb alloys onto titanium substrates.^[256,257] After etch-removal of the oxide layer they transferred the samples into a solution containing H₂PtCl₆ and according precursors for the desired alloys as well as formaldehyde as reducing agent. Subsequently the samples are heated to 180 °C for 10 hours in an autoclave leading to porous platinum film formation. The resulting electrodes showed a roughness factor of 140. In a similar procedure Yi and Co-workers used ethylene glycole as reducing agent to

fabricate PtRuIr ternary platinum nanostructures on titanium from corresponding metal salt solutions.^[258]

Platinum nanotubes can be fabricated by *template wetting*, a method combining membrane templating with electroless deposition.^[259,260] First a precursor solution film is dispensed onto the membrane and subsequently gets sucked into the pores as shown in Figure 17A. If a droplet of a low surface energy solution is dispensed on the surface of a higher surface energy porous membrane (e.g. alumina or silicon) the solution will only cover the walls of the membrane. Consequently, reduction of the precursor film results in platinum nanotube formation. Gösele and co-workers used a mixture of Pt(acac)₂ and

polylactide in CH₂Cl₂ as precursor solution.^[259] By heating the wetted membrane (macroporous silicon) to 200 °C for 24 hours Pt(acac)₂ degrades and is reduced in the presence of polylactide to metallic platinum forming particles of 8 nm in diameter. Further heating to 350 °C for one hour leads to a complete removal of polylactide and coalescence of the platinum nanoparticles to a crystallite diameter of 10 nm. After membrane removal nanotubes as shown in Figure 17B are obtained with 10 nm thick walls. Higher wall thickness or even bimetallic core-shell structures can be fabricated by a repetition of the wetting-reduction cycle.^[260]

4.4. Galvanic Replacement

The term *galvanic replacement* describes the phenomenon that less noble metals are dissolved from their surface if the surface is in contact with a metal ion solution of a more noble character which consequently deposits on top of this surface. Thus porous platinum electrodes can be generated from porous non-platinum structures and subsequent *galvanic replacement* by immersion in a platinum salt solution.

Mohl and co-workers electrodeposited nickel in presence of boric acid through an anodic aluminum oxide membrane.^[261] Subsequent immersion of the resulting nickel nanorods into a

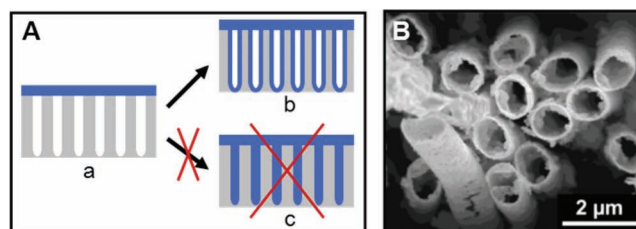


Figure 17. Fabrication of platinum nanotubes by template wetting. A: Schematic illustration of template wetting: After droplet dispensing a film is established on the membrane (a) and a thin film covers the pore walls (b), but does not completely fill the pores (c) (Graph is reproduced in the style of reference ^[260]. Copyright 2004 Wiley), B: platinum nanotubes fabricated by wetting of a porous silicon membrane with Pt(acac)₂ and polylactide and subsequent reduction of platinum at 200 °C (Reprinted with permission.^[259] Copyright 2004 American Chemical Society).

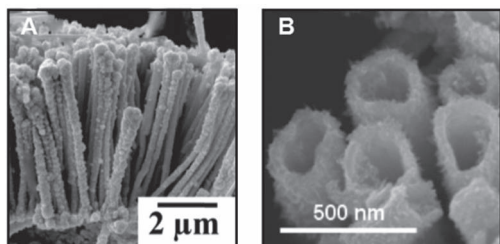


Figure 18. SEM image of Porous platinum nanorods (A) fabricated by galvanic replacement of nickel nanorods electrodeposited through a membrane template. Reprinted with permission.^[261] Copyright 2010 American Chemical Society. SEM image of hollow platinum nanotubes (B) fabricated from galvanic replacement of nickel nanorods with an H_2SO_4 pretreatment prior to replacement. Reprinted with permission.^[262] Copyright 2010 American Chemical Society.

solution of H_2PtCl_6 leads to a *galvanic replacement* of nickel with platinum. The resulting platinum nanorods (see **Figure 18A**) showed a by 57 nm larger diameter (259 ± 69 nm) compared to the sacrificial Ni-rods (202 ± 69 nm). No presence of nickel and a surface area of $30 \text{ m}^2 \text{ g}^{-1}$ were observed from XPS- and BET-analysis, respectively.

Using the same commercial anodic aluminum oxide membrane Liu and co-workers obtained hollow platinum nanotubes.^[262] Different to the procedure of Mohl and co-workers they applied a pretreatment with H_2SO_4 (0.5 mol l^{-1} , 10 min). This pretreatment induced randomly distributed defect sites on the nickel nanorods, which represent positions for preferential nickel dissolution during the galvanic replacement reaction. Consequently voids form around these positions inside the nickel structure (so called Kirkendall voids). These voids can hardly become filled by platinum deposition due to the long path for diffusive supply. Therefore nickel gets dissolved at a high rate inside of these voids and platinum is predominantly deposited at the outer surface. This spatial separation of dissolution and deposition process is supposed to enable the observed tube formation shown in **Figure 18B**. The resulting structure consists out of vertically aligned tubes of 2 μm in length, roughly 200 nm in diameter and a platinum shell thickness of 30 nm. Compared to solid platinum nanorods of the same length and diameter a by a five-fold higher surface area to mass ratio is observed for the nanotubes.

Song and co-workers deposited platinum films on single crystalline (100) silicon by galvanic deposition in HF solution (5 mol l^{-1}).^[263] In HF solution silicon is oxidized to Si^{4+} - ions which get subsequently dissolved as hexafluoride complex-ions (SiF_6^{2-}). Electrons resulting from this oxidation reaction enable the reduction of platinum ions on the silicon surface. This way they generated platinum layers consisting out of particles of 450 nm size. XRD investigation showed a

predominance of (111) orientation, indicating a face-centered cubic crystal structure. For silver films they also showed the opportunity to generate different morphologies by addition of capping agents to the deposition solution such as polyvinylpyrrolidone or polyethyleneglycole.

Chen and co-workers used photolithography based microfabrication technology in combination with galvanic replacement to fabricate arrays of hollow platinum tubes (see **Figure 19**).^[264] Fabrication starts with a silicon wafer and a 400 nm thick copper pattern. A SiO_2 layer is coated onto the wafer and subsequently plasma-etched to yield the template shown in the first pictogram in **Figure 19A**. Subsequently gold is sputtered as a conductive seed layer on the side walls. The unwanted top layer is removed by mechanical polishing (see second pictogram in **Figure 19A**). By immersion in a H_2PtCl_6 -solution for 30–180 s platinum is deposited inside the pores by galvanic replacement of the copper pattern as shown in **Figure 19B**. Subsequently the SiO_2 mask is removed in buffered HF-solution for 4–5 min. **Figure 19C** shows an electron microscopy image of the structure resulting from this process. With about 75 nm the side walls were observed to be sufficiently stable to vertically stand on the silicon wafer. Their growth during galvanic replacement reaction occurs at a rate of 1 nm s^{-1} .

4.5. Thermal Decomposition

As demonstrated by the following examples thermal decomposition (see Section 2.4) can be used for the fabrication of substrate-based electrodes in two different ways: either heating of a precursor solution on a substrate or electro spraying of precursor

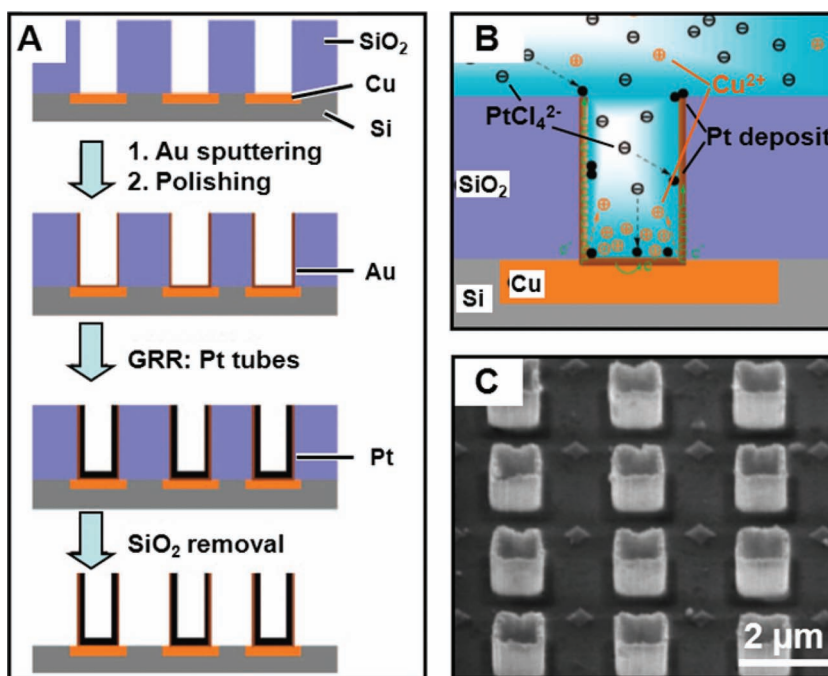


Figure 19. Fabrication of arrays of rectangular hollow platinum tubes. A: Schematic representation of the fabrication process. B: Representation of the galvanic replacement step during deposition. C: SEM image of the resulting hollow platinum tubes. Reprinted with permission.^[264] Copyright 2009 American Chemical Society.

solution onto a heated substrate. Tammeveski and co-workers deposited an ethanolic solution of H_2PtCl_6 ($5 \mu\text{l cm}^{-2}$, 3%) and boric acid onto glass slides.^[99,265] After drying, the coated glass slides were heated to 650°C to create strongly adhesive metallic films by thermal decomposition of H_2PtCl_6 . After six process repetitions these films showed a roughness factor of 22 and a film resistance of less than $2 \Omega \text{sq}^{-1}$.^[99]

Lintanf and co-workers used electrospraying technology (see 4.1.1, 4.3.3) of a precursor solution onto a preheated ceramic substrate to prepare porous platinum films for the use in automotive exhausts.^[1] Whereas the thermal decomposition of $\text{Pt}(\text{NH}_3)_4(\text{OH})_2(\text{H}_2\text{O})$ and PtCl_4 led to microporous morphology, dense films were observed with $\text{Pt}(\text{acac})_2$. A decreasing roughness of the deposited film was observed for substrate temperatures increasing from 260°C to 434°C .

4.6. Chemical Vapor Deposition (CVD)

Lo Nigro and co-workers fabricated platinum nanocolumns by metal-organic chemical vapor deposition.^[266] Their process is seedless and requires neither templates nor surfactants. Bisacetylacetonate platinum ($\text{Pt}(\text{acac})_2$) is sublimated at 170°C and moved through a horizontal reactor by a gas flow of oxygen and argon. A glass substrate is placed on a metal block which is externally heated to 250 to 550°C . After 60 min of deposition at a substrate temperature of 250 – 400°C the substrate showed to be homogeneously covered with vertically aligned platinum nanocolumns of 40 – 80 nm in diameter and $2 \mu\text{m}$ in length (see **Figure 20**). Morphology characterization by SEM and TEM showed the columns to grow along the (100)-direction and their tips to consist of (111)-planes.

4.7. Discussion

Using substrate-based electro- or electroless deposition techniques strongly adherent electrocatalysts can be established on conductive substrates. The deposition process includes catalyst formation and electrode formation in one, different to in nanoparticles based approaches. Besides electro- and electroless deposition, chemical vapor deposition (CVD) has been demonstrated to fabricate porous platinum, but CVD does not share an important advantage: low technical effort. The universal applicability of electro- and electroless techniques enable

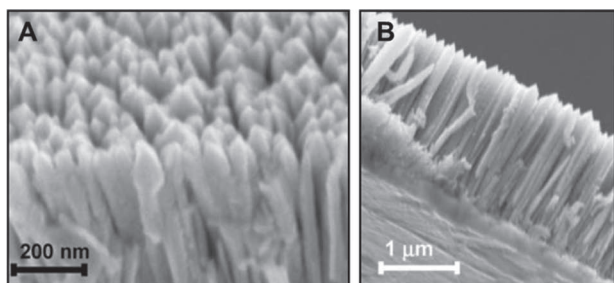


Figure 20. SEM image of platinum nanocolumns obtained by metal oxide chemical vapor deposition (MOCVD) of $\text{Pt}(\text{acac})_2$. Reprinted with permission.^[266] Copyright 2007 American Chemical Society.

catalyst formation from a huge variety of material compositions. Typically electrodes fabricated by electrodeposition have a surface roughness up to $\text{RF} = 500$. Electroless deposition techniques have also successfully been applied to structure generation with roughness factors of approximately 200. Using templating techniques during deposition, the electrocatalyst can additionally be designed in its three-dimensional structures (nanotubes, nanocolumns, ...) and thus in its material transport properties. Since the complete electrode structure is made out of platinum, a significant fraction of platinum atoms is entrapped inside the bulk and thus cannot contribute to the catalytic activity. Consequently most substrate based fabrication techniques suffer from a low platinum utilization compared to nanoparticle based or decoration approaches. A comparably high platinum utilization is obtained for hollow structures such as platinum nanotubes fabricated by e.g. template wetting or membrane templated electrodeposition. Also shape control is not as well developed as in nanoparticle synthesis (see Section 3.1.3): only some basic approaches are known. The control of surface orientation has only been shown at low surface roughness. Moreover, a relation between surface orientation and reaction selectivity in electrocatalysis has so far only been demonstrated with non-porous single crystalline electrodes.

5. Fabrication of Self-Supporting Electrodes by Dealloying

Dealloying refers to a corrosion process in which a less noble component is selectively dissolved from an alloy leaving behind a self-supporting, contiguous, nanoporous structure of a more noble component. This process has an ancient tradition: Andean people used salts and plant juices in pre-columbian times to dissolve copper and silver from the surfaces of gold-copper-silver alloys to obtain a shiny golden appearance specific for their decorative arts.^[267] Dealloying has regained attention in the last decade as technique for the fabrication of nanoporous metals with high specific surface areas.^[268–271] Characteristic for dealloyed metals is their bicontinuous ligament-channel structure, as shown in **Figure 21**. Platinum nanostructures of this kind have been created from binary metal alloys of

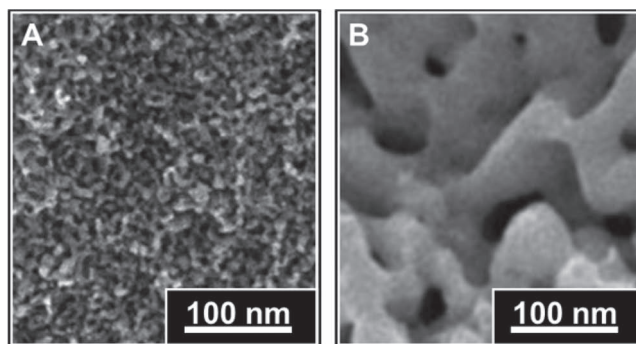


Figure 21. Electron microscopy images of a nanoporous $\text{Pt}_{80}\text{Au}_{20}$ dealloyed from $\text{Pt}_{10}\text{Au}_{10}\text{Cu}_{80}$ in concentrated HNO_3 (48 hours) before (a) and after (b) heat treatment (500°C , 15 min). Average ligament size increased from 6 nm to 50 nm during heat treatment.^[280]—Reproduced by permission of the PCCP Owner Societies.



Figure 22. Optional pathways for the fabrication of nanoporous platinum by dealloying.

Pt-Cu,^[51,52,219,270,272] Pt-Ag,^[273] Pt-Al,^[53,274] Pt-Zn^[275] and Pt-Ni,^[276] as well as Pt-Si alloys.^[277,278] Also nanoporous alloys of Pt-Au and Pt-Ni have been fabricated by dealloying utilizing ternary alloys of Pt-Au-Ag,^[26,279] Pt-Au-Cu^[280] and Pt-Ni-Si.^[281] Such dealloyed nanoporous structures are interesting for application in catalysis,^[282] [277] as well as in thermo-mechanical systems such as heat exchangers^[283] and electrochemical actuators.^[26]

In general fabrication by dealloying comprises two steps: alloying and dealloying which can both be performed in various ways as shown in **Figure 22**. The use of commercially available alloy-foils simplifies the process to the dealloying step only, and thus represents the most simple and reproducible route to fabricate nanoporous platinum. Unfortunately, the only limited range of products does not allow adjusting the alloy composition. Alloys can be either purchased from commercial manufacturers or obtained by *melting techniques*, *bilayer annealing* or *co-deposition techniques*. *Melting techniques* propose an easy variation in composition at high homogeneity, but not all laboratories have the corresponding equipment and the reproducible fabrication of according foils is not trivial to set up.^[26,269,270,272,273,279,280] *Bilayer fabrication* is based on deposition of a top-layer of one metal onto a foil of another metal by methods such as electrodeposition or physical vapor deposition (PVD). The bilayer is subsequently annealed to enable alloy formation by interdiffusion.^[53,275,276] In some cases bilayers can also be established on a substrate. To fabricate a substrate-based bimetallic film also *co-deposition methods* such as sputtering or electrodeposition can be utilized.^[219,277,278,278,284] If a free-standing structure is desired using co-deposition the substrate needs to be removable after the alloying or dealloying step. Disadvantage of bilayer and co-deposition approaches is often an only limited homogeneity. Moreover the application of thin film techniques such as sputtering and PVD is only advantageous at a low layer thickness (<1µm).

The *dealloying step* can be performed chemically by selective etching in alkaline or acidic solutions (free corrosion). For instance aluminium can be etched in 5% HCl from Pt₁₂Al₈₈ alloys.^[269]

Alternatively, during electrochemical dealloying the process is conducted under potential control offering the dealloying potential as a further parameter to influence the process (see Section 5.2).

5.1. Dealloying Mechanism

A model for the dealloying process has been derived by Erlebacher and co-workers from Monte Carlo simulations on the AgAu system.^[271,285] According to this model dealloying starts with a dissolution of a single silver atom from the flat surface of the alloy (1). This leaves behind a vacancy in the lattice and thus neighboring silver atoms become more susceptible to dissolution (2). Further dissolution occurs until the resulting cavity solely consists of a gold surface (3). Position fluctuations of gold atoms according to their surface diffusivity lead to the formation of gold clusters according to surface energy minimization, which form the later ligament structure (4). This way further silver atoms get exposed to the electrolyte which subsequently get dissolved (5).

The porosity of dealloying structures can be characterized by pore size (diameter) and ligament size (width), observed from high resolution SEM. Usually both sizes are observed to be in the same range and thus only one is listed as characteristic length scale or feature size λ (see **Figure 23** for typical values).

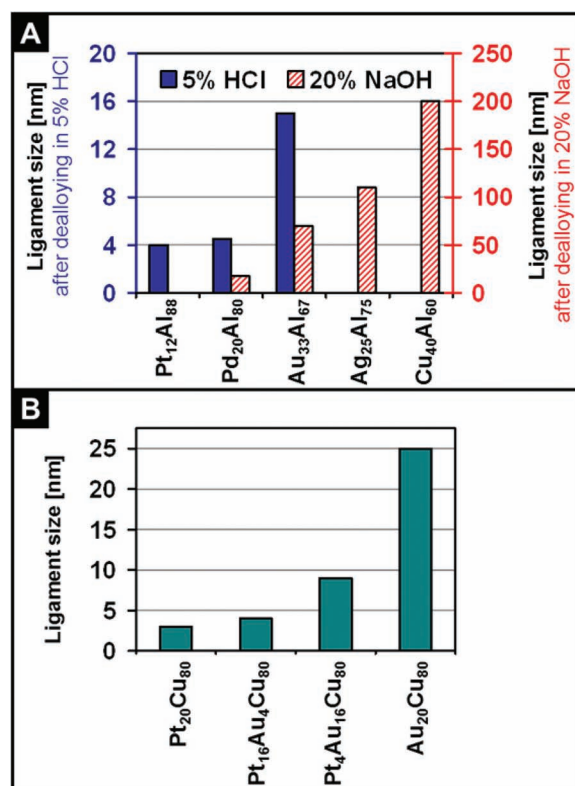


Figure 23. Ligament size dependencies of different dealloying systems. A Ligament sizes of different noble metal–aluminum alloys with dealloying in either 5% HCl or 20% NaOH (graph is created on basis of data reference [269]). B Ligament sizes of platinum-gold-copper alloys with varying platinum and copper content (graph is created on basis of data from reference [280]).

As a consequence of the discussed dealloying model by Erlebacher and co-workers this length scale evolves from a balance of the dissolution rate (k_{diss}) of the less noble component and the surface diffusion (k_{SD}). Based on their simulations they suggested the following relation:

$$\lambda \propto \left(\frac{k_{\text{SD}}}{k_{\text{diss}}} \right)^{\frac{1}{6}} \quad (7)$$

For some dealloyed structures residues of the less noble metals can still be detected by EDX after dealloying. This is a consequence of slow surface diffusion of the noble metal leading to an incomplete dealloying. Consequently an enclosure of fractions of the less noble metal partner is observed forming a core-shell like structure (alloy core, noble metal shell).^[279,286]

5.2. Parting Limit and Critical Potential

Besides the characteristic length scale two thresholds are characteristic for the dealloying of each alloy: *parting limit* and *critical potential*. The *parting limit* represents the minimum fraction of the less noble component in the alloy to enable dealloying. Below the parting limit the outermost layers of the less noble metal get dissolved but no reorganization of the more noble metal takes place.^[270,271,285,287] This is also described as passivation.

The *critical potential* represents the electrode potential threshold which has to be overcome in order to enable dissolution of the less noble component from the alloy compound. The critical potential is very sensitive to the exact composition. For instance an increase of about 24 mV in critical potential per at.-% Cu was observed for PtCu alloys.^[272] For determination of the critical dealloying potential either one *potential sweep* or several *potential hold experiments* have to be performed.^[272]

Figure 24 shows *potential sweep experiments* run with PtCu alloys of different composition. The first current peak indicates an initial dissolution of surface copper and saturates when all surface copper is dissolved (passivation region). The charge corresponding to this first peak is nearly independent of the exact alloy composition. Higher potentials are required for copper dissolution from inside the PtCu-alloy (dealloying): The critical dealloying potential is thus indicated by the beginning of the second increase in current. Increasing critical potentials and lower dealloying current densities are observed with decreasing copper content from comparison of Cu₈₀Pt₂₀ (0.605 V vs. NHE), Cu₇₅Pt₂₅ (0.750 V vs. NHE), and Cu₇₁Pt₂₉ (0.815 V vs. NHE).

Figure 25 shows *potential hold experiments* of a Cu₇₅Pt₂₅ alloy. Here the electrode is held at a specific potential and the current is observed over time. At 0.730 V vs. NHE the current immediately decreases after application of the potential. Additional dealloying currents are observed for higher dissolution potentials. This clear transition in the current-time response observable between 0.730 and 0.792 V vs. NHE indicates the critical dealloying potential of this specific alloy system. Compared to potential sweep experiments, potential hold experiments are more elaborate since several experiments and thus several samples are required to find the transition in curve progression

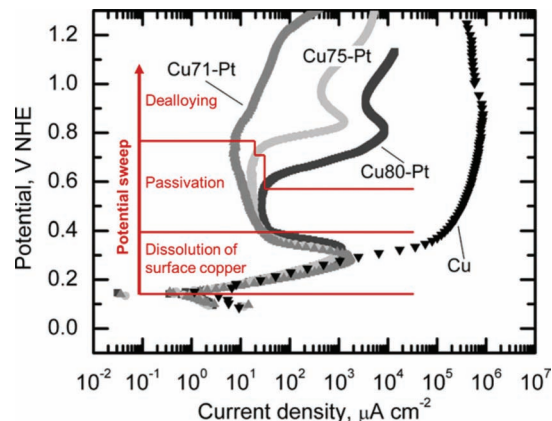


Figure 24. Determination of critical dealloying potential of Cu-Pt alloys by potential sweeps in N₂ deaerated H₂SO₄ (1 mol l⁻¹). Curve progression shows three potential regions: dissolution of surface copper, passivation and dealloying. Potential sweeps were performed starting from open circuit potential at a scan rate of 1 mV s⁻¹ and 10 mV s⁻¹ for alloy samples and the pure copper sample, respectively. Reproduced with permission.^[272] Copyright 2005 ECS.

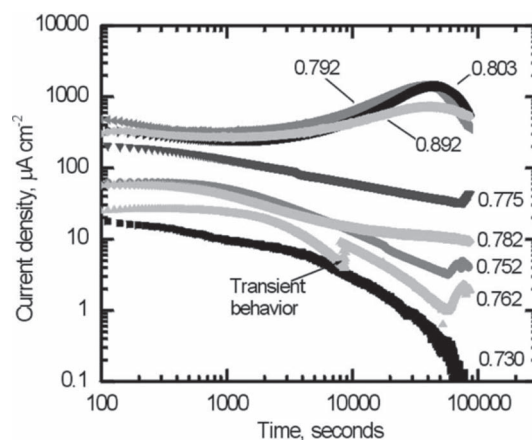


Figure 25. Determination of critical dealloying potential of a Cu₇₅Pt₂₅ alloy by potential hold experiments in N₂ deaerated H₂SO₄ (1 mol l⁻¹). For each curve the corresponding dissolution potentials (in V vs. NHE) is indicated in the graph. Each curve is recorded with a new sample. Reproduced with permission.^[272] Copyright 2005 ECS.

indicating the critical potential. The advantage of potential hold experiments is their higher precision according to the sharp transition in curve progression.

5.3. Controlling Pore and Ligament Size

In consistence with the discussed mechanism (Section 5.1) several parameters were experimentally proven to influence the resulting pore and ligament size during fabrication: choice of noble metal component, dealloying solution, and dealloying potential. For different noble metals M in M-Al alloys a trend towards larger ligament size is observed from Pt, Pd to Au to Ag to Cu (see Figure 23A). This trend reflects the role of the surface diffusivity in equation (7): The smaller the surface diffusivity of the noble metal, the smaller the ligament size.^[269]

Similar results were observed from a comparison of copper alloys of gold ($\text{Au}_{20}\text{Cu}_{80}$) and platinum ($\text{Au}_{20}\text{Pt}_{80}$): Here the significantly higher surface diffusivity of gold ($10^{-19} \text{ cm}^2 \text{ s}^{-1}$)^[285] compared to platinum ($10^{-22} \text{ cm}^2 \text{ s}^{-1}$)^[285] leads to a ligament size of about 25 nm, about 7 times higher than observed for dealloyed $\text{Pt}_{20}\text{Cu}_{80}$.^[272,280] Already small fractions of platinum doped into AuAg-alloys show a significant reduction of the characteristic length from 10–20 nm down to only 4 nm (see also PtAuCu-system in Figure 23B).^[279] Consequently, a 3–4 times higher BET-surface area is measured for the doped compared to the non-doped AuAg.^[279]

Zhang and co-workers dealloyed palladium and gold alloys of aluminium chemically in 5% HCl and 20% NaOH.^[269] What they observed were significantly larger pore/ligament sizes when using 5% HCl (see Figure 23A). Consequently, they concluded the presence of Cl^- -ions to accelerate surface diffusivity.

In electrochemical dealloying, the choice of potential can be used to adjust the etching rate k_{diss} and thus according to equation (7) to adjust ligament sizes.^[288,289] For instance Parida and co-workers observed the ligament/channel size in their dealloyed AuAg to decrease from 20 nm to 4 nm if the dealloying potential is increased from 600 mV to 850 mV vs. Ag/AgCl in $1 \text{ mol l}^{-1} \text{ HClO}_4$.^[289]

A further opportunity to increase the pore and ligament size is to perform a post fabrication heat treatment (see Figure 21).^[280,290] The elevated temperatures lead to coarsening of the ligaments enabled by strongly enhanced surface diffusivity of the atoms.^[280,290] This way the feature size can be increased from a few nanometers up to hundred nanometers and even micrometer scale.

5.4. Alternative Dealloying Techniques

5.4.1. Repetition of Alloying-Dealloying

In a two-step modification of dealloying, a hierarchical pore system has been created by alloying and dealloying of an already dealloyed nanoporous gold.^[291] The resulting structure comprises pores of 150 nm as backbone (from first dealloying) and porous structure of 15 nm width at the skin (from second dealloying) of the backbone pores.

5.4.2. Electrochemical Alloying-Dealloying

An electrochemical alloying-dealloying strategy has been proposed by Liu and co-workers.^[219] In a two-step process they first potentiostatically co-deposited a PtCu alloy followed by anodic dealloying of copper from the alloy. This way porous platinum films have been fabricated with roughness factors of 700. In a further modification cyclic voltammetry scans were performed in an acidic solution of H_2PtCl_6 and CuSO_4 .^[51,52] This way within every cycle co-deposition and copper dissolution is alternated. A defined regulation of the surface roughness has been shown depending on the number of deposition cycles. Roughness factors of higher than $\text{RF} = 3000$ were achieved using this technique.

5.5. Discussion

If there exists a commercial foil of the desired composition which can get chemically dealloyed, this represents the easiest and fastest fabrication approach to porous platinum electrodes of all strategies. Unfortunately this is usually not the case. In particular in research, alloy composition variations are required, since the alloy composition predefines most of the properties of the later porous structure such as parting limit, critical dealloying potential and ligament size. Therefore alloy formation is the key step in dealloying. Another critical point is the ligament size which is predefined by alloy-composition and the surface diffusion of the noble metal content. An enlargement of the ligament and pore size of dealloyed structures has been shown by heat treatment, but the underlying coarsening occurs very fast and thus is not easy to control. Another possible way to obtain dealloying structures impossible to fabricate with platinum is to dealloy another metal and subsequently decorate the surface with a thin film of platinum as discussed in Section 6.

6. Platinum Decoration of Porous Metal Electrodes

In this Section fabrication techniques are presented that in particular qualify for the decoration of an already porous conductive structure (*base structure*), what means to cover its surface with a thin layer of platinum at a thickness ranging from submonolayer to a few monolayers. In particular corresponding methods should enable a homogeneous decoration. This is a non-trivial task, since most methods rely on diffusive mass transport and thus concentration gradients inside the pore structure will cause a preferential deposition at the outer compared to inner ranges of the base structure. Moreover to homogeneity, methods differ in their applicability on different porous structures and their opportunities to vary as well as to control the layer thickness.

There are several reasons why the decoration of a base structure of another metal with a thin layer of platinum can be an advantageous fabrication strategy for porous platinum electrodes such as costs, fabrication technique limitations and catalytic properties. Low costs compared to previously discussed methods are attributed to decoration due to high platinum utilization. Nearly all of the deposited platinum atoms in the decoration layer are placed at the surface and thus contribute to the catalytic activity of the electrode.^[292]

Another reason for choosing a decoration based strategy is that some fabrication approaches cannot be performed with platinum itself. In such cases the desired method can be performed with another metal suitable to the fabrication process followed by surface decoration with platinum. This way it is possible to nevertheless run such methods and to make use of their advantages and specific structure geometries for the fabrication of porous platinum electrodes. For instance, bubble templating is not possible during platinum deposition.^[293,294] To use largely grown bubbles as template, bubble generation during deposition has to be limited to the substrate and should not occur on the deposit. This is for instance possible with copper deposition on a gold substrate according to the high

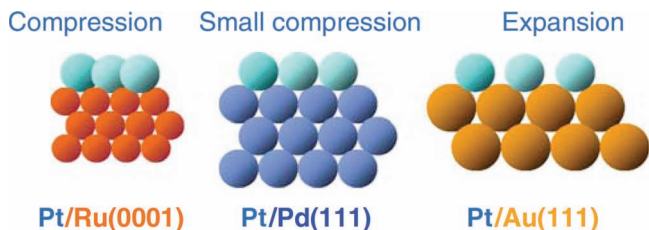


Figure 26. Schematic illustration of the substrate induced shift in interatomic distances of platinum adlayers (monolayer thickness) on exemplary substrate surfaces of ruthenium, palladium and gold. Reproduced with permission.^[292] Copyright 2007 Springer.

overpotential of copper for hydrogen generation compared to on gold. This way copper can easily grow into the resulting voids between the bubbles. Such a spatial process separation is impossible during platinum deposition. Electrochemical surface reorganization protocols known for the fabrication of porous gold electrodes represent another technique which cannot directly be performed with platinum.^[29,295,296] Also here, decoration with platinum was demonstrated to be a valuable alternative strategy to anyway use these protocols for the generation of porous platinum.^[29,295] Moreover, the decoration of structures resulting from dealloying (see Section 5) can be interesting: For each noble metal, the achievable pore geometry and ligament size is limited to a certain range predefined by the metal's surface diffusivity. By decoration of dealloyed non-platinum alloys also other pore geometries and ranges in ligament size can be fabricated, which are impossible to obtain by dealloying from platinum based alloys.^[269,282,297]

Furthermore, beneficial catalytic effects are observed for platinum layers of only submonolayer to a few monolayer thickness.^[292,298,299] If only present in a few monolayers the atoms of the adlayer have different interatomic distances compared to in pure platinum electrodes induced by the substrate lattice as shown in **Figure 26**. This leads to a shift in d-band filling and thus to deviant catalytic properties from bulk platinum.^[292,300] Moreover to catalytic activity they also observed an enhanced stability of the catalyst for such decorated systems during potential cycling.^[301] This stabilization effect is also supposed to be a consequence of the d-band modification.^[301,302]

6.1. Pt-Electrodeposition

There are several examples showing the electrodeposition of a few monolayer equivalents of platinum onto surfaces of other metals.^[29,295] Nevertheless it is not at all a trivial challenge to homogeneously decorate a porous structure by means of electrodeposition, since electrodeposition relies on diffusive reactant supply. Accordingly a concentration gradient develops during deposition inside the pores preventing homogenous decoration coverage over the complete pore system of the electrode. Consequently, most deposition will occur at the outmost part of

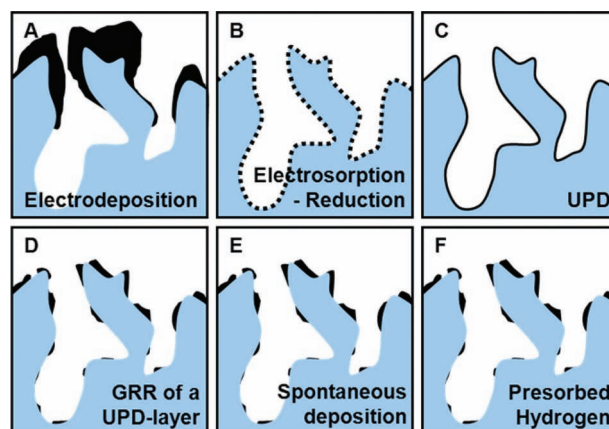


Figure 27. Schematic illustration of the expected decoration coverage on an exemplary porous base structure using different decoration methods. The undecorated base structure is depicted in blue, the decoration layer in black.

the porous structure (see **Figure 27A**). One idea to circumvent the development of a significant concentration gradient is to let soak the porous structure in the electrolyte long time before deposition.^[303] This way a homogeneous initial concentration inside the structure can be established. During deposition a pulse scheme or cycles alternating deposition and waiting time can be applied to enable concentration relaxation (see Section 4.1.4,^[229,303]). This way Zhang and co-workers fabricated a platinum decorated electrode from dealloyed $\text{Au}_{42}\text{Ag}_{58}$ with a platinum surface area of $150 \text{ m}^2 \text{ g}^{-1}$ ($353 \text{ cm}^2 \text{ Pt per cm}^2$ of footprint area).^[303]

Electrosorption-reduction is a modification to standard electrodeposition techniques enabling a homogeneous decoration, consisting of a surface-limited *electrosorption* step and a subsequent *reduction* step as shown in **Figure 28**.^[230,231,304] In a realization of this method, Zhao and co-workers performed cyclic voltammetry scans between e.g. 0.3 and 1.3 V vs. Ag/AgCl to irreversibly oxidize the planar Pt(II)-complex on the surface of carbon nanotubes to an octahedral Pt(IV)-complex (*electrosorption*). Subsequently the electrode was transferred into 0.1 mol l^{-1}

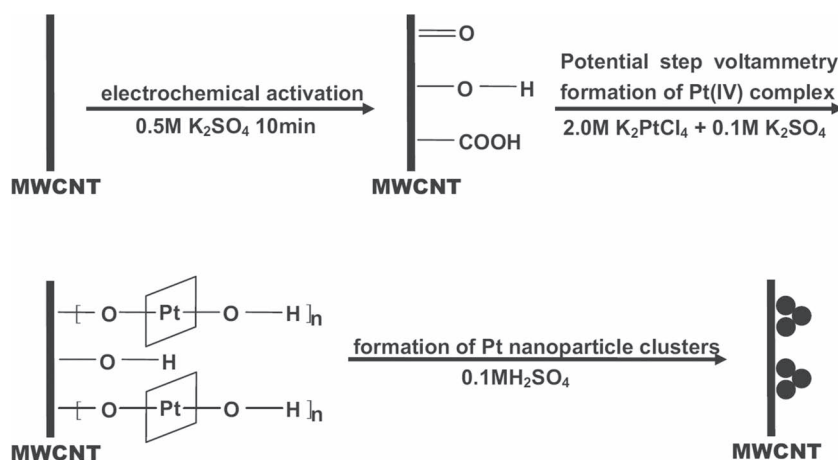


Figure 28. Schematic illustration of platinum deposition on carbon nanotubes (MWCNT) by first MWCNT activation, Pt(II) electroadsorption and final platinum reduction according to nanoparticle clusters. Reproduced with permission.^[231]

H₂SO₄ (no platinum salt in solution) and was subjected to further cyclic voltammetry scans with an extended negative scan limit (e.g. 100 mV s⁻¹, -0.25 and 1.30 V vs. Ag/AgCl). During these scans reduction of the adsorbed Pt(IV) complexes to a zero-valent platinum occurs resulting in a decoration of the carbon nanotube substrate with an active surface area of 71 m² g⁻¹ Pt.^[231] Since the *electrosorption* process saturates after covering all accessible absorption sites, also the subsequent deposition is limited by the previous adsorption sites. This way a homogeneous distribution of platinum can be assured, even over the surface of a porous base structure. The decoration is limited to one monolayer equivalent. Nevertheless, the decoration is not expected to form a continuous layer but clusters caused by an energy-lowering surface reorganization after deposition as depicted in Figure 27B. To our knowledge, the application of this decoration strategy has yet only been shown on carbon. Thus it remains unclear whether a similar adsorption behavior can be found on base structures made out of materials other than carbon.

6.2. Under Potential Deposition and Galvanic Replacement

For some metals the deposition of a monolayer onto specific crystal surfaces of another metal is enabled at electrode potentials more oxidative than the redox-potential of the bulk deposition. This phenomenon is called underpotential deposition (UPD).^[73,305] This coverage is thermodynamically driven by a reduction in the interfacial energy of the electrode surface towards the electrolyte. Since UPD only leads to a reduction in interfacial energy for a deposition of up to one monolayer, deposition by UPD is thermodynamically limited to the decoration with one monolayer. Moreover this limitation intrinsically leads to a homogeneous distribution of the adlayer over the entire electrode surface as shown in Figure 27C. UPD of metals such as copper or bismuth on platinum are well known.^[105,251,306] Unfortunately platinum itself does only show UPD behavior on only few metal surfaces (e.g. on Au(111)) and thus UPD can in most cases not directly be used for platinum decoration.^[306]

As workaround an indirect UPD-strategy has become very popular in the last years which uses the galvanic replacement of an UPD-deposited monolayer of copper (UPD-monolayer replacement).^[247,292,307–310] Here, a monolayer of copper is deposited by UPD on the surface of a noble metal base structure. Subsequently the electrode is dipped into a solution containing platinum ions, resulting in a galvanic replacement of copper by platinum as schematically shown in **Figure 29** (also see Section 4.4). The exchange proceeds in accordance to the relation of transferred electrons in the dissolution and deposition reaction. This means two copper adatoms have to be dissolved to deposit platinum from one [Pt(IV)Cl₆]²⁻ ion. Copper is chosen as sacrificial metal in most cases since it shows UPD behavior on most crystallographic planes of gold, palladium and others.^[306] To generate a higher decoration thickness than equivalent to one UPD monolayer of copper this process can be repeated for several times.^[307] This strategy can be applied to nanoparticle based electrodes as well as substrate-based or self-supporting electrode structures. Moreover this strategy can

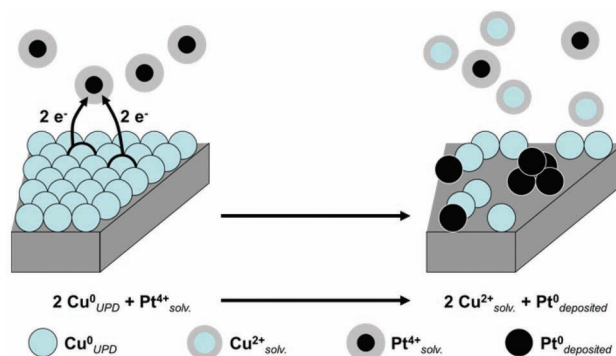


Figure 29. Schematic representation of galvanic replacement of a copper monolayer deposited via UPD on a gold electrode by platinum. This graph has been newly prepared in the style of reference [307].

also be used in the reverse direction: to decorate platinum with other metals such as gold.^[301]

Compared to UPD, only a limited homogeneity of the adatom distribution can be achieved with galvanic replacement. Different to the surface area limited deposition in UPD, the replacement reaction is not specific to surface sites. The dissolution of copper atoms and deposition of platinum do not necessarily occur in close vicinity to each other since electron transfer between dissolution and deposition reaction can proceed through the electrode. Platinum supply occurs via diffusive transport and thus deposition of platinum inside the pores is disadvantaged compared to the outer ranges of the base structure. Therefore the deposited platinum atoms do not necessarily cover the former adsorption sites of the UPD monolayer and the deposited platinum arranges in randomly distributed and sized clusters, with a preference to the outer ranges of the pore structure (see Figure 27D).^[292,301,307] Accordingly to the same reason Liu and co-workers observed larger diameters on the top than on the bottom of their platinum nanotubes fabricated by galvanic replacement.^[262]

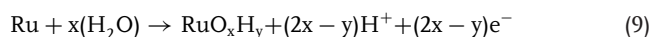
Following the approach of replacement of a copper UPD-monolayer Mkwizu and co-workers fabricated bimetallic multilayer electrodes.^[311] Starting from a glassy carbon disc they deposited a layer of copper by UPD which subsequently was replaced with platinum or ruthenium by a galvanic replacement reaction in a corresponding precursor solution. By repetition of copper UPD and galvanic replacement they stacked monolayers of platinum and ruthenium on top of each other (substrate-Pt-Ru-Pt-Ru-...). For methanol oxidation they found superior electrocatalytic activity for such sequentially stacked monolayers of platinum and ruthenium compared to codeposited platinum-ruthenium alloys or pure platinum.

In case of non-noble metals the deposition of a copper monolayer is not required to enable galvanic replacement. Accordingly, Papadimitriou and co-workers fabricated platinum electrodes starting from thin layers of copper, iron, cobalt and nickel by galvanic replacement in a platinum solution. Different to in Section 4.4 the replacement reaction was stopped before all nickel was dissolved to end up with a decoration layer rather than an expensive structure completely made of platinum.^[312–314]

6.3. Spontaneous Deposition

Spontaneous deposition of up to a few monolayers of platinum has been observed by immersion of a non-oxidized metal surface (e.g. ruthenium) in a solution containing platinum salts.^[315,316] In a typical procedure the electrode is first transferred into its completely reduced state by either high-temperature gas phase treatment (argon sputtering and vacuum oven at 1400 °C) or by application of a reduction potential.^[315,317] During immersion the electrode is oxidized during a simultaneous reduction of platinum ions driven by a difference in redox-potential (e.g. between $[\text{PtCl}_6]^{4-}/\text{Pt}$ and $\text{RuO}_x\text{H}_y/\text{Ru}$).^[316,318] In that respect, spontaneous deposition is comparable to galvanic replacement. But in contrast to galvanic replacement no less-noble metal is dissolved during oxidation of the electrode substrate. The deposition stops when the electrode substrate is completely oxidized. Hence, spontaneous deposition does neither rely on the application of an external potential nor a chemical reducing agent. Platinum decoration has successfully been demonstrated on ruthenium, gold and highly ordered pyrolytic graphite.^[308,315–318]

On ruthenium substrates the following reactions are expected to occur:^[318]



Resulting deposits of platinum spontaneously deposited on single crystalline ruthenium Ru(0001) consist of small clusters/nanoparticles.^[316] These clusters are of uniform size and homogeneously dispersed over the entire surface. In case of a porous structure a similar inhomogeneous distribution is expected for spontaneous deposition as resulting from galvanic replacement suffering from concentration gradients (see Figure 27E). Surface coverages of more than 10 monolayers were proven to be possible with spontaneous deposition.^[314] The number of monolayer equivalents deposited during deposition was observed to depend on immersion time and the concentration of the platinum ions in solution.

6.4. Electroless Deposition

In standard electroless deposition concentration gradients in the supply of precursor and reducing agent lead to an inhomogeneous decoration, comparable to in electrodeposition.

Table 1. Comparison of methods for the decoration of porous metal electrodes with platinum. (Rating scale: ++ = very good choice, + = good choice, 0 = feasible, - = difficult choice).

Properties	Electrodeposition	Electrosorption-reduction	UPD	UPD-monolayer replacement	Spontaneous deposition	Electroless deposition	Presorbed hydrogen
Universal applicability	++	-	0 a)	+	0 ^{b)}	++	+
Limitation of deposition thickness	0	++ ^{b)}	++ ^{b,c)}	+ ^{c,d)}	+	-	+ ^{d)}
Homogeneous decoration	0 ^{e)}	++	++	+ ^{e)}	+ ^{e)}	- ^{e)}	+ ^{e)}

^{a)}depends on the crystallographic planes/ elements; ^{b)}surface site specific thermodynamic limit; ^{c)}limited to a monolayer equivalent; ^{d)}deposition thickness can be increased by process repetition; ^{e)}less homogeneous on porous electrodes due to diffusive precursor supply.

Moreover thickness control is a critical issue, since the reaction is impossible to stop once the pores have been soaked with precursor and reducing agent.

The use of *presorbed hydrogen* represents a possible modification to achieve a thin decoration by electroless decoration. This approach consists of two steps: hydrogen generation and sample immersion in H_2PtCl_6 -solution.^[319] Previous to exposure to the metal precursor hydrogen is either generated on the electrode by exposure to NaBH_4 (15 min) or by a reduction pulse (10 min at -0.6 V vs. Ag/AgCl). This way fractions of the generated hydrogen get sorbed inside the microstructure. When subsequently immersed in a H_2PtCl_6 -solution, platinum ions were reduced by the sorbed hydrogen on the surface of the gold microstructure resulting in a platinum decoration. Since platinum ions are supplied diffusively a similar inhomogeneous distribution has to be expected as with galvanic replacement and spontaneous deposition (see Figure 27F). Similar procedures have been applied for the decoration of platinum electrodes with other metals such as gold and ruthenium.^[320,321]

6.5. Discussion

Decoration of an already porous electrode base structure is a non-trivial issue but can be a valuable alternative to creating a porous structure out of platinum, since decoration enables high platinum utilization. Moreover the electronic structure of such decoration layers can be advantageously varied compared to pure platinum leading to improvements in terms of catalytic activity or stability. The difficulty of this strategy remains the homogeneous decoration inside a porous structure.

Table 1 compares the strengths of the discussed methods for platinum decoration of porous base structures made of materials other than platinum. Electro- and electroless deposition represent methods of universal applicability, since their applicability does not strongly depend on the substrate surface. Different to this UPD and spontaneous deposition of platinum are only observed on specific crystallographic planes of a few metals. Since UPD is thermodynamically limited to a coverage of one monolayer, UPD enables a homogeneous decoration without cluster formation. Following the approaches of galvanic replacement of a UPD-monolayer, spontaneous deposition or electroless deposition by presorbed hydrogen the deposition process is limited by the pretreatment. This means the deposition is stopped when the UPD-monolayer, zero-valent metal or presorbed hydrogen is consumed. Nevertheless this does not

Table 2. Strengths and weaknesses of the different strategies for the fabrication of porous platinum electrodes. (Rating scale: ++ = very good choice, + = good choice, 0 = feasible, - = difficult choice, ne = not evaluable).

Method	Deposition of NP-ink	Nanoparticle networks	Electrodeposition	Electroless Deposition	Dealloying from commercial foils	Dealloying including alloy formation	Decoration of non-Pt metals
Section	3.4.1	3.4.2	4.1	4.2	5	5	6
Generation of RF = 30	+ ^{a)}	0	++	++	- ^{b)}	+ ^{b)}	++ ^{c)}
Generation of RF = 300	++ ^{a)}	+	++	++	0 ^{b)}	++ ^{b)}	++ ^{c)}
Generation of RF = 3000	++ ^{a)}	-	+ ^{d)}	-	++ ^{b)}	++ ^{b)}	+ ^{c)}
Scalability of RF	++	0	++	+	0	+	-
High Pt-utilization	++	++	0	0	0	0	++
Applicability to Pt alloys	++	0/-	0	++	-	0	++
Low technical effort	+	++	0	++	++	0	0
Low time consumption	0	+	++	+	++	0	++
Micro-scale applications	0	ne	++	++	0	+	+
Large-scale applications	++	ne	+	+	+	+	+
High quantity fabrication	++	++	0	++	+	+	0

^{a)}strongly depends on the applied layer thickness but can exceed 5000; ^{b)}is defined by alloy composition and foil thickness; ^{c)}surface roughness is predefined by the base structure; ^{d)}only known in combination with dealloying.

guarantee a homogeneous layer, since with these methods the sites of platinum deposition are not predefined. Consequently, clusters are formed during these deposition processes and diffusive supply of platinum precursor leads to a preferential platinum deposition in the outer range of the porous base structures. Electrodeposition and electroless deposition neither have an intrinsic process stop nor does deposition occur on predefined positions. Thus these methods enable deposition of thick layers, but at a comparably lower homogeneity; in particular in porous structures where diffusion and electric field gradients play a crucial role.

Conclusion

In this article four basic strategies for the fabrication of porous platinum electrodes with numerous modifications have been discussed: nanoparticle based electrode fabrication, substrate based electrode fabrication, dealloying and decoration. **Table 2** compares strength and weakness of selected fabrication pathways.

Electrodes can be fabricated in relevant ranges in surface roughness by using ink-deposition of nanoparticles or electrodeposition. Scalability in surface roughness is achieved by adjusting the thickness of the deposited ink and deposition charge, respectively. Electroless deposition techniques in principle enable a variation in surface roughness e.g. by variation of deposition time or the availability of precursor applied during synthesis, but roughness factors of 1000 and higher have not been reported to our knowledge. In nanoparticle network formation the achievable dimensions are related to the formation mechanism and can thus only be scaled in a limited range. Surface roughness factors obtained by dealloying range from 20 to more than 3000. Since in dealloying the surface roughness is predefined by the utilized alloy, a change in alloy fabrication is required for surface roughness variation. An increase in ligament/pore size and thus

a decrease in surface roughness can also be obtained by a heat treatment as discussed in Section 5.3. Decoration techniques can be applied on base structures of low as well as of high porosity, whereas homogeneous decoration becomes more challenging with increasing surface roughness (see Section 6). A scaling in surface roughness cannot be achieved by decoration itself, since these methods are intended to only generate coverage of up to only a few monolayer equivalents.

A *high platinum utilization* can in particular be achieved using decoration and nanoparticle based approaches, since nearly all platinum atoms are located at the surface and thus can contribute to the catalytic activity of the electrode. In case of substrate-based and self-supporting strategies a significant fraction of platinum atoms is entrapped inside the bulk without contact to the electrode-electrolyte interface.

In nanoparticle synthesis *platinum alloy electrodes* can be fabricated by addition of a further metal precursors following the same approaches as for monometallic platinum electrodes. In case of nanoparticle network formation a change in the composition of the nanoparticles can disable the network formation mechanism. Electrochemical or electroless co-deposition is not possible for all kinds of desired alloys, but for most alloys relevant to electrocatalysis. Nanoporous platinum alloys from dealloying have already been shown for e.g. PtAu. To fabricate binary alloys by dealloying, ternary alloys are required as starting material with a sufficiently high fraction of the sacrificial element. Besides these bulky alloy structures, multi-metallic surfaces can be generated by decoration with platinum and other metals. Such electrodes can show high catalytic activity and high structural stability as discussed in Section 6.

Concerning *technical effort* dealloying from commercial alloy-foils represent the most simple method to fabricate highly porous platinum electrodes. If no commercial foils are available, alloy fabrication makes the dealloying method significantly more elaborate. Other simple methods in respect to technical

effort are: nanoparticle networks and electroless deposition since in their simplest form they only require a reaction vessel and according chemicals. Ink-deposition techniques require spraying or casting devices, electrodeposition and in most cases also decoration require a potentiostat, equipment which is usually present in electrochemical laboratories. Moreover the use of a potentiostat can be an advantage concerning process control since it enables to monitor and steer the process from external.

Electrodeposition, dealloying from already prepared foils and decoration in principle feature *low time consumption* which is in the range of an hour. Some electroless deposition techniques such as hydrothermal synthesis proceed on a timescale of a few hours to a day. Similar process times are required for nanoparticle formation. Network formation does not significantly increase process duration, whereas ink formation, ink deposition and drying require additional time. Dealloying can require more than 2 days, if time required for alloy formation is included in this estimate.

In *micro-scale applications* in particular electroless deposition and electrodeposition become interesting since these techniques can precisely be applied on conductive areas pre-defined by microfabrication techniques such as optical lithography. The same is true for dealloying of alloys formed by electrodeposition, co-sputtering or similar techniques that enable an area selective deposition and alloy formation. Here co-sputtering is advantageous to annealing of a bilayer since high temperatures can lead to an incompatibility with other process elements (e.g. electronic elements in close vicinity). The application of dealloyed foils and ink deposition is very difficult on the micrometer scale according to handling problems during shaping and integration of such layers. Nevertheless ink deposition represents a state of the art techniques besides electrodeposition in small scale applications as for instance in the fabrication of micro fuel cells.^[322] In applications in μm -scale such as in stimulation electrodes only physical vapor deposition (thermal evaporation or sputtering) techniques leading to comparably smooth surface areas are applied besides electrodeposition.^[22–24]

In *large-scale applications* such as PEM fuel cell electrodes thin film technology (nanoparticle synthesis followed by ink deposition) represents the state of the art since nanoparticle synthesis can occur in a batch process and homogeneous layers can be fabricated on the scale of square meters using spraying and casting technology.^[68] Moreover such electrodes can be operated at a comparably low platinum utilization (e.g. by dispersion on cheap support materials).^[10] Electrodeposition is not that present in large scale realizations compared to nanoparticle synthesis, most probably referring from higher costs according to the more expansive equipment compared to ink-technology and high power consumption. Another disadvantage in case of electrodeposition is the requirement of accordingly large current sources. Nevertheless electrodeposition and also electroless deposition are considered as promising replacement of currently used physical vapor deposition for the generation of counter electrodes in dye-sensitized solar cells. Here these techniques benefit from good properties in terms of catalytic activity and optical reflectivity as well as from lower fabrication costs compared to state of the art. Dealloying

on a large scale does not differ from on standard lab scale, but suffers from low platinum utilization resulting in high material costs.

For industrial *fabrication at high quantity*, nanoparticle based strategies benefit from an easy implementation of nanoparticle synthesis as batch process. Dealloying could be performed at high throughput by using on large foils that are continuously driven through a dealloying solution. Processes requiring the handling of several single pieces as during electrical connection procedures, required for electrodeposition or decoration methods, reduce the fabrication throughput.

7. Perspective

With limited fossil fuel reserves and the increasing world energy demand alternative energy conversion approaches such as fuel cells are expected to play a key role in our future energy economy. Accordingly, there will be an increasing demand for porous platinum electrodes and their *industrial realization* of the various fabrication approaches will get more into focus. While some fabrication concepts such as nanoparticle networks are in a very early stage and their strengths and applicability are still unproven, other methods such as the deposition of nanoparticle inks have already shown their general applicability even at large scale.

Nevertheless, state of the art porous platinum electrodes are still too expensive for mass production. Hence one key task is to further increase *platinum utilization*. Here size and shape control as well as methods such as decoration techniques or hollow nanoparticles will play an important role. Lower platinum loadings can also be achieved by *alloy-electrocatalysts*, which in addition can help to *enhance poisoning resistance and long-term stability*. Here a deeper mechanistic understanding of the interactions between alloying partners on the atomic scale is required to design optimum catalysts. Thereto the interactions at atomic scale should be investigated by experiments on model structures accompanied by simulations. Based on this knowledge, the next challenge will be to transfer the desired atomic arrangements into three-dimensional, porous structures and to *adapt their fabrication to industrial scales*.

In particular the development of electrochemical sensors with an increased signal to noise ratio may benefit from progress in shape controlled fabrication. According methods allow for the fabrication of electrocatalysts with predominant crystallographic orientations, which in turn can promote specific reaction pathways while suppressing parallel reactions. Today this *reaction specificity* has only been demonstrated in chemical catalysis, the demonstration in electrochemical applications is still pending. Shape controlled fabrication by nanoparticle synthesis in solution is already well established, whereas shape controlled fabrication by electrodeposition is still a challenge. Key problem in electrochemical fabrication is to deposit catalyst particles of strict crystallographic orientation in close vicinity of each other. Therefore corresponding electrodes lack in an only low surface area and surface roughness, respectively. Here, future work has to show whether shape control and surface roughness remain contradictory and whether a realization at application relevant scale is possible.

ACKNOWLEDGEMENTS

We gratefully acknowledge financial support from the German Research Association DFG (GR 1322).

Received: June 10, 2011

Revised: August 15, 2011

Published online: October 5, 2011

- [1] A. Lintanf, R. Neagu, E. Djurado, *Solid State Ionics* **2007**, *177*, 3491.
- [2] L. M. Bronstein, *Colloid Chem.* **2003**, *226*, 55.
- [3] C. Kim, H. Lee, *Catal. Comm.* **2009**, *11*, 7.
- [4] G. A. Somorjai, Y. M. Li, *Top. Catal.* **2010**, *53*, 832.
- [5] C. A. Witham, W. Y. Huang, C. K. Tsung, J. N. Kuhn, G. A. Somorjai, F. D. Toste, *Nat. Chem.* **2010**, *2*, 36.
- [6] T. K. Sau, A. L. Rogach, F. Jackel, T. A. Klar, J. Feldmann, *Adv. Mater.* **2010**, *22*, 1805.
- [7] S. Ikeda, S. Ishino, T. Harada, N. Okamoto, T. Sakata, H. Mori, S. Kuwabata, T. Torimoto, M. Matsumura, *Angew. Chem., Int. Ed.* **2006**, *45*, 7063.
- [8] B. C. H. Steele, A. Heinzel, *Nature* **2001**, *414*, 345.
- [9] S. Kerzenmacher, J. Ducrée, R. Zengerle, F. von Stetten, *J. Power Sources* **2008**, *182*, 1.
- [10] J. Larminie, A. Dicks, *Fuel Cell Systems Explained*, John Wiley & Sons, Ltd, Chichester, England **2000**.
- [11] X. Y. Zhang, W. Lu, J. Y. Da, H. T. Wang, D. Y. Zhao, P. A. Webley, *Chem. Commun.* **2009**, 195.
- [12] *Handbook of Fuel Cells - Fundamentals, Technology, Applications; VOLUME2: ELECTROCATALYSIS*, John Wiley & Sons **2003**.
- [13] H. Huang, W. K. Zhang, M. C. Li, Y. P. Gan, J. H. Chen, Y. F. Kuang, *J. Colloid Interface Sci.* **2005**, *284*, 593.
- [14] M. Maja, C. Orecchia, M. Strano, P. Tosco, M. Vanni, *Electrochim. Acta* **2000**, *46*, 423.
- [15] F. W. Campbell, R. G. Compton, *Anal. Bioanal. Chem.* **2010**, *396*, 241.
- [16] Y. Y. Song, D. Zhang, W. Gao, X. H. Xia, *Chem.- Eur. J.* **2005**, *11*, 2177.
- [17] J. H. Yuan, K. Wang, X. H. Xia, *Adv. Funct. Mat.* **2005**, *15*, 803.
- [18] M. H. Yang, F. L. Qu, Y. S. Lu, Y. He, G. L. Shen, R. Q. Yu, *Biomaterials* **2006**, *27*, 5944.
- [19] Y. Bai, Y. Y. Sun, C. Q. Sun, *Biosens. Bioelectron.* **2008**, *24*, 579.
- [20] G. Korotcenkov, S. Do Han, J. R. Stetter, *Chem. Rev.* **2009**, *109*, 1402.
- [21] B. Pejčić, P. Eadington, A. Ross, *Environ. Sci. Technol.* **2007**, *41*, 6333.
- [22] K. C. Cheung, *Biomed. Microdevices* **2007**, *9*, 923.
- [23] A. C. R. Grayson, R. S. Shawgo, A. M. Johnson, N. T. Flynn, L. I. Yawen, M. J. Cima, R. Langer, *Proc. IEEE* **2004**, *92*, 6.
- [24] S. Mailley, M. Hyland, P. Mailley, J. A. McLaughlin, E. T. McAdams, *Bioelectrochemistry* **2004**, *63*, 359.
- [25] E. M. Hudak, J. T. Mortimer, H. B. Martin, *J. Neural Eng.* **2010**, *7*.
- [26] H. J. Jin, X. L. Wang, S. Parida, K. Wang, M. Seo, J. Weissmuller, *Nano Lett.* **2010**, *10*, 187.
- [27] E. Antolini, T. Lopes, E. R. Gonzalez, *J. Alloys Compd.* **2008**, *461*, 253.
- [28] C. Coutanceau, A. F. Rakotondrainibe, A. Lima, E. Garnier, S. Pronier, J. M. Leger, C. Lamy, *J. Appl. Electrochem.* **2004**, *34*, 61.
- [29] J. B. Jia, L. Y. Cao, Z. H. Wang, *Langmuir* **2008**, *24*, 5932.
- [30] N. Kristian, Y. L. Yu, P. Gunawan, R. Xu, W. Q. Deng, X. W. Liu, X. Wang, *Electrochim. Acta* **2009**, *54*, 4916.
- [31] H. F. Wang, Z. P. Liu, *J. Am. Chem. Soc.* **2008**, *130*, 10996.
- [32] <http://www.platinum.matthey.com/pgm-prices/price-charts/>, in **2010**.
- [33] J. Y. Chen, B. Lim, E. P. Lee, Y. N. Xia, *Nano Today* **2009**, *4*, 81.
- [34] Y. Xia, Y. J. Xiong, B. Lim, S. E. Skrabalak, *Angew. Chem. Int. Ed.* **2009**, *48*, 60.
- [35] J. H. Choi, K. J. Jeong, Y. Dong, J. Han, T. H. Lim, J. S. Lee, Y. E. Sung, *J. Power Sources* **2006**, *163*, 71.
- [36] N. M. Markovic, P. N. Ross, *Surf. Sci. Rep.* **2002**, *45*, 121.
- [37] N. M. Markovic, H. A. Gasteiger, P. N. Ross, X. D. Jiang, I. Villegas, M. J. Weaver, *Electrochim. Acta* **1995**, *40*, 91.
- [38] J. S. Spendelow, A. Wieckowski, *Phys. Chem. Chem. Phys.* **2004**, *6*, 5094.
- [39] T. Iwasita, *Electrochim. Acta* **2002**, *47*, 3663.
- [40] E. Antolini, *Mater. Chem. Phys.* **2003**, *78*, 563.
- [41] Y. J. Lee, D. J. Park, J. Y. Park, *IEEE Sens. J.* **2008**, *8*, 1922.
- [42] L. Yuan, M. H. Yang, F. L. Qu, G. L. Shen, R. Q. Yu, *Electrochim. Acta* **2008**, *53*, 3559.
- [43] D. Rathod, C. Dickinson, D. Egan, E. Dempsey, *Sens. Actuators, B* **2010**, *143*, 547.
- [44] J. J. Li, R. Yuan, Y. Q. Chai, X. Che, W. J. Li, X. Zhong, *Microchim. Acta* **2011**, *172*, 163.
- [45] J. Noh, S. Park, H. Boo, H. C. Kim, T. D. Chung, *Lab Chip* **2011**, *11*, 664.
- [46] Y. J. Lee, J. Y. Park, *J. Kor. Phys. Soc.* **2011**, *58*, 1505.
- [47] Y. J. Lee, J. Y. Park, Y. Kim, J. W. Ko, *Curr. Appl. Phys.* **2011**, *11*, 211.
- [48] P. Miao, M. Shen, L. Ning, G. Chen, Y. Yin, *Anal. Bioanal. Chem.* **2011**, *399*, 2407.
- [49] Y. Tang, G. P. Kotchey, H. Vedala, A. Star, *Electronanl.* **2011**, *23*.
- [50] P. Jacquinet, B. Muller, B. Wehrli, P. C. Hauser, *Anal. Chim. Acta* **2001**, *432*, 1.
- [51] A. Kloke, C. Köhler, R. Zengerle, S. Kerzenmacher, F. von Stetten, "Reaction specific platinum electrodes for implantable glucose fuel cells: versatile fabrication by cyclic electrodeposition", presented at PowerMEMS. 2010, Leuven, Belgium, **2010**, 73.
- [52] A. Kloke, S. Kerzenmacher, R. Zengerle, F. von Stetten, "Facile Fabrication of Ultra Porous Platinum Electrodes and Their Application for Energy Harvesting Glucose Fuel Cells", presented at ECS 215th Meeting - San Francisco CA, USA, **2009**, 572.
- [53] S. Kerzenmacher, U. Kräling, M. Schroeder, R. Brämer, R. Zengerle, F. von Stetten, *J. Power Sources* **2010**, *195*, 6524.
- [54] M. Nazeeruddin, E. Baranoff, M. Grätzel, *Solar Energy* **2011**, *85*, 1172.
- [55] S. J. Cho, J. Y. Ouyang, *J. Phys. Chem. C* **2011**, *115*, 8519.
- [56] C. Y. Lin, J. Y. Lin, C. C. Wan, T. C. Wei, *Electrochim. Acta* **2011**, *56*, 1941.
- [57] G. Calogero, P. Calandra, A. Irrera, A. Sinopoli, I. Citro, G. Di Marco, *Energy Environ. Sci.* **2011**, *4*, 1838.
- [58] K. Sun, B. H. Fan, J. Y. Ouyang, *J. Phys. Chem. C* **2010**, *114*, 4237.
- [59] C. M. Chen, C. H. Chen, S. J. Cherng, T. C. Wei, *Mater. Chem. Phys.* **2010**, *124*, 173.
- [60] Y. L. Lee, C. L. Chen, L. W. Chong, C. H. Chen, Y. F. Liu, C. F. Chi, *Electrochem. Commun.* **2010**, *12*, 1662.
- [61] Z. M. Peng, H. Yang, *Nano Today* **2009**, *4*, 143.
- [62] A. R. Tao, S. Habas, P. D. Yang, *Small* **2008**, *4*, 310.
- [63] C. Burda, X. B. Chen, R. Narayanan, M. A. El-Sayed, *Chem. Rev.* **2005**, *105*, 1025.
- [64] T. K. Sau, A. L. Rogach, *Adv. Mater.* **2010**, *22*, 1781.
- [65] C. R. K. Rao, D. C. Trivedi, *Coord. Chem. Rev.* **2005**, *249*, 613.
- [66] M. Sakamoto, M. Fujistuka, T. Majima, *J. Photochem. Photobiol. C* **2009**, *10*, 33.
- [67] J. H. Bang, K. S. Suslick, *Adv. Mater.* **2010**, *22*, 1039.
- [68] S. Litster, G. McLean, *J. Power Sources* **2004**, *130*, 61.
- [69] V. Mehta, J. S. Cooper, *J. Power Sources* **2003**, *114*, 32.
- [70] J. H. Wee, K. Y. Lee, S. H. Kim, *J. Power Sources* **2007**, *165*, 667.
- [71] A. C. Chen, P. Holt-Hindle, *Chem. Rev.* **2010**, *110*, 3767.
- [72] C. R. K. Rao, M. Pushpavanam, *Mater. Chem. Phys.* **2001**, *68*, 62.

- [73] M. Paunovic, M. Schlesinger, *Fundamentals of electrochemical deposition*, Wiley, New York 2006.
- [74] R. Strey, P. E. Wagner, Y. Viisanen, *J. Phys. Chem.* **1994**, *98*, 7748.
- [75] E. E. Finney, R. G. Finke, *J. Colloid Interface Sci.* **2008**, *317*, 351.
- [76] R. Becker, W. Döring, *Annalen der Physik* **1935**, *416*, 719.
- [77] J. C. Hulthen, C. R. Martin, *J. Mater. Chem.* **1997**, *7*, 1075.
- [78] A. Henglein, M. Giersig, *J. Phys. Chem. B* **2000**, *104*, 6767.
- [79] A. Henglein, B. G. Ershov, M. Malow, *J. Phys. Chem.* **1995**, *99*, 14129.
- [80] C. W. Chen, T. Takezako, K. Yamamoto, T. Serizawa, M. Akashi, *Colloids Surf. A* **2000**, *169*, 107.
- [81] L. T. Bai, H. Z. Zhu, J. S. Thrasher, S. C. Street, *ACS Appl. Mater. Interfaces.* **2009**, *1*, 2304.
- [82] Y. Wang, X. Xu, Z. Q. Tian, Y. Zong, H. M. Cheng, C. J. Lin, *Chem.-Eur. J.* **2006**, *12*, 2542.
- [83] J. Y. Chen, T. Herricks, Y. N. Xia, *Angew. Chem., Int. Ed.* **2005**, *44*, 2589.
- [84] X. S. Peng, K. Koczur, S. Nigro, A. C. Chen, *Chem. Commun.* **2004**, 2872.
- [85] S. Komarneni, D. S. Li, B. Newalkar, H. Katsuki, A. S. Bhalla, *Langmuir* **2002**, *18*, 5959.
- [86] W. X. Tu, H. F. Lin, *Chem. Mater.* **2000**, *12*, 564.
- [87] Z. L. Liu, J. Y. Lee, W. X. Chen, M. Han, L. M. Gan, *Langmuir* **2004**, *20*, 181.
- [88] V. K. Lamer, R. H. Dinegar, *J. Amer. Chem. Soc.* **1950**, *72*, 4847.
- [89] L. C. Ciacchi, W. Pompe, A. De Vita, *J. Amer. Chem. Soc.* **2001**, *123*, 7371.
- [90] L. C. Ciacchi, W. Pompe, A. De Vita, *J. Phys. Chem. B* **2003**, *107*, 1755.
- [91] M. A. Watzky, R. G. Finke, *J. Amer. Chem. Soc.* **1997**, *119*, 10382.
- [92] Y. J. Song, W. A. Steen, D. Pena, Y. B. Jiang, C. J. Medforth, Q. S. Huo, J. L. Pincus, Y. Qiu, D. Y. Sasaki, J. E. Miller, J. A. Shelnuttt, *Chem. Mater.* **2006**, *18*, 2335.
- [93] Y. J. Song, Y. Yang, C. J. Medforth, E. Pereira, A. K. Singh, H. F. Xu, Y. B. Jiang, C. J. Brinker, F. van Swol, J. A. Shelnuttt, *J. Amer. Chem. Soc.* **2004**, *126*, 635.
- [94] R. M. Garcia, Y. J. Song, R. M. Dorin, H. R. Wang, P. Li, Y. Qiu, F. van Swol, J. A. Shelnuttt, *Chem. Commun.* **2008**, 2535.
- [95] J. Belloni, M. Mostafavi, H. Remita, J. L. Marignier, M. O. Delcourt, *New J. Chem.* **1998**, *22*, 1239.
- [96] G. Surendran, L. Ramos, B. Pansu, E. Prouzet, P. Beaunier, F. Audonnet, H. Remita, *Chem. Mater.* **2007**, *19*, 5045.
- [97] Y. Mizukoshi, R. Oshima, Y. Maeda, Y. Nagata, *Langmuir* **1999**, *15*, 2733.
- [98] D. M. Calderon, U. Morales, C. Velasquez, V. H. Lara, L. Salgado, *Catal. Lett.* **2009**, *132*, 268.
- [99] K. Tammeveski, T. Tenno, J. Niinisto, T. Leitner, G. Friedbacher, L. Niinisto, *Appl. Surf. Sci.* **2000**, *156*, 135.
- [100] J. O. Hernandez, E. A. Choren, *Thermochim. Acta* **1983**, *71*, 265.
- [101] D. Vollath, *Nanomaterials: An Introduction to Synthesis, Properties and Application*, Wiley-VCH, Weinheim 2008.
- [102] J. Luo, M. M. Maye, V. Petkov, N. N. Kariuki, L. Y. Wang, P. Njoki, D. Mott, Y. Lln, C. J. Zhong, *Chem. Mater.* **2005**, *17*, 3086.
- [103] X. W. Teng, X. Y. Liang, S. Maksimuk, H. Yang, *Small* **2006**, *2*, 249.
- [104] S. Trasatti, O. A. Petrii, *J. Electroanal. Chem.* **1992**, *327*, 353.
- [105] C. L. Green, A. Kucernak, *J. Phys. Chem. B* **2002**, *106*, 1036.
- [106] S. Brimaud, C. Coutanceau, E. Garnier, J. M. Leger, F. Gerard, S. Pronier, M. Leoni, *J. Electroanal. Chem.* **2007**, *602*, 226.
- [107] S. Brunauer, P. H. Emmett, E. Teller, *J. Amer. Chem. Soc.* **1938**, *60*, 309.
- [108] C. G. Schull, *J. Amer. Chem. Soc.* **1948**, *70*, 1405.
- [109] Y. K. Choi, G. Wang, M. H. Nayfeh, S. T. Yau, *Biosens. Bioelectron.* **2009**, *24*, 3103.
- [110] B. Liu, H. Y. Li, L. Die, X. H. Zhang, Z. Fan, J. H. Chen, *J. Power Sources* **2009**, *186*, 62.
- [111] R. W. J. Scott, A. K. Datye, R. M. Crooks, *J. Amer. Chem. Soc.* **2003**, *125*, 3708.
- [112] J. Solla-Gullon, V. Montiel, A. Aldaz, J. Clavilier, *J. Electrochem. Soc.* **2003**, *150*, E104-E109.
- [113] K. W. Wang, C. T. Yeh, *J. Colloid Interface Sci.* **2008**, *325*, 203.
- [114] A. Habrioux, E. Sibert, K. Servat, W. Vogel, K. B. Kokoh, N. Alonso-Vante, *J. Phys. Chem. B* **2007**, *111*, 10329.
- [115] J. Luo, M. M. Maye, V. Petkov, N. N. Kariuki, L. Y. Wang, P. Njoki, D. Mott, Y. Lln, C. J. Zhong, *Chem. Mater.* **2005**, *17*, 3086.
- [116] D. I. Garcia-Gutierrez, C. E. Gutierrez-Wing, L. Giovanetti, J. M. Ramallo-Lopez, F. G. Requejo, M. Jose-Yacaman, *J. Phys. Chem. B* **2005**, *109*, 3813.
- [117] J. Yin, J. H. Wang, T. Zhang, X. D. Wang, *Catal. Lett.* **2008**, *125*, 76.
- [118] K. E. Elkins, T. S. Vedantam, J. P. Liu, H. Zeng, S. H. Sun, Y. Ding, Z. L. Wang, *Nano Lett.* **2003**, *3*, 1647.
- [119] W. H. Wang, X. L. Tian, K. Chen, G. Y. Cao, *Colloids Surf. A* **2006**, *273*, 35.
- [120] J. D. Aiken, R. G. Finke, *J. Mol. Catal. A* **1999**, *145*, 1.
- [121] Y. Sun, L. Zhuang, J. Lu, X. Hong, P. Liu, *J. Amer. Chem. Soc.* **2007**, *129*, 15465+.
- [122] T. Frelink, W. Visscher, J. A. R. Vanveen, *J. Electroanal. Chem.* **1995**, *382*, 65.
- [123] K. Yamamoto, T. Imaoka, W. J. Chun, O. Enoki, H. Katoh, M. Takenaga, A. Sono, *Nat. Chem.* **2009**, *1*, 397.
- [124] H. Ye, J. A. Crooks, R. M. Crooks, *Langmuir* **2007**, *23*, 11901.
- [125] J. M. Petroski, Z. L. Wang, T. C. Green, M. A. El-Sayed, *J. Phys. Chem. B* **1998**, *102*, 3316.
- [126] S. B. Han, Y. J. Song, J. M. Lee, J. Y. Kim, D. H. Kim, K. W. Park, *Bull. Korean Chem. Soc.* **2009**, *30*, 2362.
- [127] M. Subhramannia, V. K. Pillai, *J. Mater. Chem.* **2008**, *18*, 5858.
- [128] G. A. Somorjai, J. Y. Park, *Angew. Chem., Int. Ed.* **2008**, *47*, 9212.
- [129] S. S. Cheong, J. D. Watt, R. D. Tilley, *Nanoscale* **2010**, *2*, 2045.
- [130] G. A. Somorjai, D. W. Blakely, *Nature* **1975**, *258*, 580.
- [131] K. M. Bratlie, H. Lee, K. Komvopoulos, P. D. Yang, G. A. Somorjai, *Nano Lett.* **2007**, *7*, 3097.
- [132] I. Lee, R. Morales, M. A. Albiter, F. Zaera, *Proc. Nat. Acad. Sci. U.S.A.* **2008**, *105*, 15241.
- [133] T. S. Ahmadi, Z. L. Wang, T. C. Green, A. Henglein, M. A. ElSayed, *Science* **1996**, *272*, 1924.
- [134] Y. N. Wu, S. J. Liao, Z. X. Liang, L. J. Yang, R. F. Wang, *J. Power Sources* **2009**, *194*, 805.
- [135] A. Henglein, *J. Phys. Chem. B* **2000**, *104*, 2201.
- [136] L. H. Lu, G. Y. Sun, H. J. Zhang, H. S. Wang, S. Q. Xi, J. Q. Hu, Z. Q. Tian, R. Chen, *J. Mater. Chem.* **2004**, *14*, 1005.
- [137] J. H. Zeng, J. Yang, J. Y. Lee, W. J. Zhou, *J. Phys. Chem. B* **2006**, *110*, 24606.
- [138] O. A. Petrii, *J. Solid State Electrochem.* **2008**, *12*, 609.
- [139] S. Alayoglu, A. U. Nilekar, M. Mavrikakis, B. Eichhorn, *Nat. Mater.* **2008**, *7*, 333.
- [140] Z. Peng, J. Wu, H. Yang, *Chem. Mater.* **2010**, *22*, 1098.
- [141] S. E. Habas, H. Lee, V. Radmilovic, G. A. Somorjai, P. Yang, *Nat. Mater.* **2007**, *6*, 692.
- [142] H. P. Liang, H. M. Zhang, J. S. Hu, Y. G. Guo, L. J. Wan, C. L. Bai, *Angew. Chem., Int. Ed.* **2004**, *43*, 1540.
- [143] Y. G. Sun, B. T. Mayers, Y. N. Xia, *Nano Lett.* **2002**, *2*, 481.
- [144] X. W. Lou, L. A. Archer, Z. C. Yang, *Adv. Mater.* **2008**, *20*, 3987.
- [145] Y. G. Sun, Y. A. Xia, *Nano Lett.* **2003**, *3*, 1569.
- [146] L. H. Lu, G. Y. Sun, S. Q. Xi, H. S. Wang, H. J. Zhang, T. D. Wang, X. H. Zhou, *Langmuir* **2003**, *19*, 3074.
- [147] J. Wang, K. P. Loh, Y. L. Zhong, M. Lin, J. Ding, Y. L. Foo, *Chem. Mater.* **2007**, *19*, 2566.
- [148] Y. G. Sun, Y. N. Xia, *Science* **2002**, *298*, 2176.
- [149] X. Q. Huang, H. H. Zhang, C. Y. Guo, Z. Y. Zhou, N. F. Zheng, *Angew. Chem., Int. Ed.* **2009**, *48*, 4808.

- [150] K. S. Choi, E. W. McFarland, G. D. Stucky, *Adv. Mater.* **2003**, *15*, 2018.
- [151] M. A. Lopez-Quintela, *Curr. Op. Colloid Interface Sci.* **2003**, *8*, 137.
- [152] G. S. Attard, C. G. Goltner, J. M. Corker, S. Henke, R. H. Templer, *Angew. Chem., Int. Ed.* **1997**, *36*, 1315.
- [153] T. Kijima, T. Yoshimura, M. Uota, T. Ikeda, D. Fujikawa, S. Mouri, S. Uoyama, *Angew. Chem., Int. Ed.* **2004**, *43*, 228.
- [154] M. P. Pileni, *Nat. Mater.* **2003**, *2*, 145.
- [155] J. Solla-Gullon, V. Montiel, A. Aldaz, J. Clavilier, *J. Electroanal. Chem.* **2000**, *491*, 69.
- [156] Y. J. Song, R. M. Garcia, R. M. Dorin, H. R. Wang, Y. Qiu, J. A. Shelnett, *Angew. Chem., Int. Ed.* **2006**, *45*, 8126.
- [157] G. Surendran, G. Apostolescu, M. Tokumoto, E. Prouzet, L. Ramos, P. Beaunier, P. J. Kooyman, A. Etcheberry, H. Remita, *Small* **2005**, *1*, 964.
- [158] A. Walcarius, *Anal. Bioanal. Chem.* **2010**, *396*, 261.
- [159] X. J. Guo, C. M. Yang, P. H. Liu, M. H. Cheng, K. J. Chao, *Crys. Growth Des.* **2005**, *5*, 33.
- [160] A. Fukuoka, H. Araki, J. Kimura, Y. Sakamoto, T. Higuchi, N. Sugimoto, S. Inagaki, M. Ichikawa, *J. Mater. Chem.* **2004**, *14*, 752.
- [161] A. Fukuoka, H. Araki, Y. Sakamoto, N. Sugimoto, H. Tsukada, Y. Kumai, Y. Akimoto, M. Ichikawa, *Nano Lett.* **2002**, *2*, 793.
- [162] M. Q. Zhao, L. Sun, R. M. Crooks, *J. Amer. Chem. Soc.* **1998**, *120*, 4877.
- [163] M. Platt, R. A. W. Dryfe, E. P. L. Roberts, *Electrochim. Acta* **2004**, *49*, 3937.
- [164] M. Platt, R. A. W. Dryfe, *Phys. Chem. Chem. Phys.* **2005**, *7*, 1807.
- [165] A. Trojanek, J. Langmaier, Z. Samec, *J. Electroanal. Chem.* **2007**, *599*, 160.
- [166] R. A. W. Dryfe, *Phys. Chem. Chem. Phys.* **2006**, *8*, 1869.
- [167] C. N. R. Rao, G. U. Kulkarni, P. J. Thomas, V. V. Agrawal, P. Saravanan, *J. Phys. Chem. B* **2003**, *107*, 7391.
- [168] J. H. Bang, K. S. Suslick, *Adv. Mater.* **2010**, *22*, 1039.
- [169] R. Basnayake, Z. R. Li, S. Katar, W. Zhou, H. Rivera, E. S. Smotkin, D. J. Casadonte, C. Korzeniewski, *Langmuir* **2006**, *22*, 10446.
- [170] V. Saez, T. J. Mason, *Molecules* **2009**, *14*, 4284.
- [171] Q. M. Shen, L. P. Jiang, H. Zhang, Q. H. Min, W. H. Hou, J. J. Zhu, *J. Phys. Chem. C* **2008**, *112*, 16385.
- [172] A. Quintanilla, M. Valvo, U. Lafont, E. M. Kelder, M. T. Kreutzer, F. Kapteijn, *Chem. Mater.* **2010**, *22*, 1656.
- [173] A. Jaworek, A. T. Sobczyk, *J. Electrostatics* **2008**, *66*, 197.
- [174] J. van Erven, R. Moerman, J. C. M. Marijnissen, *Aerosol Sci. Technol.* **2005**, *39*, 941.
- [175] F. Mafune, J. Y. Kohno, Y. Takeda, T. Kondow, *J. Phys. Chem. B* **2003**, *107*, 4218.
- [176] Z. J. Yan, R. Q. Bao, D. B. Chrisey, *Nanotechnology* **2010**, *21*.
- [177] W. T. Nichols, T. Sasaki, N. Koshizaki, *J. Appl. Phys.* **2006**, *100*, 114911.
- [178] W. T. Nichols, T. Sasaki, N. Koshizaki, *J. Appl. Phys.* **2006**, *100*, 114912.
- [179] W. T. Nichols, T. Sasaki, N. Koshizaki, *J. Appl. Phys.* **2006**, *100*, 114913.
- [180] V. Amendola, M. Meneghetti, *Phys. Chem. Chem. Phys.* **2009**, *11*, 3805.
- [181] E. Antolini, *J. Mater. Sci.* **2003**, *38*, 2995.
- [182] S. H. Sun, F. Jaouen, J. P. Dodelet, *Adv. Mater.* **2008**, *20*, 3900.
- [183] S. J. Guo, D. Wen, Y. M. Zhai, S. J. Dong, E. K. Wang, *ACS Nano* **2010**, *4*, 3959.
- [184] M. Sakthivel, A. Schlange, U. Kunz, T. Turek, *J. Power Sources* **2010**, *195*, 7083.
- [185] J. Ryu, H. S. Kim, H. T. Hahn, D. Lashmore, *Biosens. Bioelectron.* **2010**, *25*, 1603.
- [186] S. H. Joo, S. J. Choi, I. Oh, J. Kwak, Z. Liu, O. Terasaki, R. Ryoo, *Nature* **2001**, *412*, 169.
- [187] L. Wang, Y. Yamauchi, *Chem. Mater.* **1911**, *21*, 3562.
- [188] F. Schulz, S. Franzka, G. Schmid, *Adv. Funct. Mater.* **2002**, *12*, 532.
- [189] S. Martin, P. L. Garcia-Ybarra, J. L. Castillo, *J. Power Sources* **2010**, *195*, 2443.
- [190] X. Leimin, L. Shijun, Y. Lijun, L. Zhenxing, *Fuel Cells* **2009**, *9*, 101.
- [191] M. S. Wilson, J. A. Valerio, S. Gottesfeld, *Electrochim. Acta* **1995**, *40*, 355.
- [192] M. S. Wilson, *US Patent* **5,234,777**, **1993**.
- [193] D. P. Wilkinson, J. J. Zhang, R. Hui, J. Fergus, X. G. Li, *Proton Exchange Membrane Fuel Cells: Materials Properties and Performance*, CRC Press, Taylor and Francis Group, Boca Raton FL **2010**.
- [194] Y. Y. Shao, J. Liu, Y. Wang, Y. H. Lin, *J. Mater. Chem.* **2009**, *19*, 46.
- [195] J. Marie, R. Chenitz, M. Chatenet, S. Berthon-Fabry, N. Cornet, P. Achard, *J. Power Sources* **2009**, *190*, 423.
- [196] J. H. Kim, B. Fang, M. Kim, J. S. Yu, *Catal. Today* **2009**, *146*, 25.
- [197] J. H. Kim, B. Fang, S. B. Yoon, J. S. Yu, *Appl. Catal. B* **2009**, *88*, 368.
- [198] B. Z. Fang, J. H. Kim, M. Kim, J. S. Yu, *Chem. Mater.* **2009**, *21*, 789.
- [199] C. Wang, M. Waje, X. Wang, J. M. Tang, R. C. Haddon, Y. S. Yan, *Nano Lett.* **2004**, *4*, 345.
- [200] J. Prabhuram, T. S. Zhao, Z. K. Tang, R. Chen, Z. X. Liang, *J. Phys. Chem. B* **2006**, *110*, 5245.
- [201] R. Klajn, T. P. Gray, P. J. Wesson, B. D. Myers, V. P. Dravid, S. K. Smoukov, B. A. Grzybowski, *Adv. Funct. Mater.* **2008**, *18*, 2763.
- [202] G. Ramanath, J. Arcy-Gall, T. Maddanimath, A. V. Ellis, P. G. Ganesan, R. Goswami, A. Kumar, K. Vijayamohan, *Langmuir* **2004**, *20*, 5583.
- [203] F. Mafune, J. Kohno, Y. Takeda, T. Kondow, *J. Phys. Chem. B* **2003**, *107*, 12589.
- [204] J. P. Xie, Q. B. Zhang, W. J. Zhou, J. Y. Lee, D. I. C. Wang, *Langmuir* **2009**, *25*, 6454.
- [205] G. Franc, E. Badetti, V. Colliere, J. P. Majoral, R. M. Sebastian, A. M. Caminade, *Nanoscale* **2009**, *1*, 233.
- [206] Y. K. Park, S. H. Yoo, S. Park, *Langmuir* **2008**, *24*, 4370.
- [207] D. Yang, S. Sun, H. Meng, J. P. Dodelet, E. Sacher, *Chem. Mater.* **2008**, *20*, 4677.
- [208] F. Mafune, J. Kohno, Y. Takeda, T. Kondow, *J. Amer. Chem. Soc.* **2003**, *125*, 1686.
- [209] A. M. Feltham, M. Spiro, *Chem. Rev.* **1971**, *71*, 177.
- [210] R. M. Penner, *J. Phys. Chem. B* **2002**, *106*, 3339.
- [211] C. M. Chen, C. H. Chen, T. C. Wei, *Electrochim. Acta* **2010**, *55*, 1687.
- [212] Y. H. Hong, Y. C. Tsai, *J. Nanomaterials* **2009**, 892178.
- [213] J. S. Ye, H. F. Cui, Y. Wen, W. D. Zhang, G. Q. Xu, F. S. Sheu, *Microchim. Acta* **2006**, *152*, 267.
- [214] I. Gonzalez-Gonzalez, E. R. Fachini, A. A. Scibioh, D. A. Tryk, M. Tague, H. D. Abruna, C. R. Cabrera, *Langmuir* **2009**, *25*, 10329.
- [215] W. Tang, S. Jayaraman, T. F. Jaramillo, G. D. Stucky, E. W. McFarland, *J. Phys. Chem. C* **2009**, *113*, 5014.
- [216] S. Toyama, M. Someya, O. Takei, T. Ohtake, R. Usami, K. Horikoshi, Y. Ikariyama, *Chem. Lett.* **2001**, 160.
- [217] J. M. Sieben, M. M. E. Duarte, C. E. Mayer, *J. Appl. Electrochem.* **2008**, *38*, 483.
- [218] J. Obert, S. B. Lalvani, *J. Appl. Electrochem.* **2004**, *34*, 397.
- [219] H. T. Liu, P. He, Z. Y. Li, J. H. Li, *Nanotechnology* **2006**, *17*, 2167.
- [220] H. Liu, F. Favier, K. Ng, M. P. Zach, R. M. Penner, *Electrochim. Acta* **2001**, *47*, 671.
- [221] M. M. E. Duarte, A. S. Pilla, J. M. Sieben, C. E. Mayer, *Electrochem. Commun.* **2006**, *8*, 159.
- [222] M. C. Tsai, T. K. Yeh, C. H. Tsai, *Mater. Chem. Phys.* **2008**, *109*, 422.

- [223] F. Ye, L. Chen, J. J. Li, J. L. Li, X. D. Wang, *Electrochem. Commun.* **2008**, *10*, 476.
- [224] N. Tian, Z. Y. Zhou, S. G. Sun, Y. Ding, Z. L. Wang, *Science* **2007**, *316*, 732.
- [225] N. Tian, Z. Y. Zhou, S. G. Sun, *J. Phys. Chem. C* **2008**, *112*, 19801.
- [226] T. W. Zhu, N. Tian, D. W. Kong, S. G. Sun, *Science in China Series B-Chemistry* **2009**, *52*, 1660.
- [227] N. Tian, Z. Y. Zhou, N. F. Yu, L. Y. Wang, S. G. Sun, *J. Amer. Chem. Soc.* **2010**, *132*, 7580.
- [228] Z. Y. Zhou, Z. Z. Huang, D. J. Chen, Q. Wang, N. Tian, S. G. Sun, *Angew. Chem., Int. Ed.* **2010**, *49*, 411.
- [229] H. S. Kim, N. P. Subramanian, B. N. Popov, *J. Power Sources* **2004**, *138*, 14.
- [230] Y. Zhao, L. H. Fan, H. H. Zhong, Y. F. Li, *Microchim. Acta* **2007**, *158*, 327.
- [231] Y. Zhao, L. Z. Fan, H. Z. Zhong, Y. F. Li, S. H. Yang, *Adv. Funct. Mater.* **2007**, *17*, 1537.
- [232] J. A. Bennett, Y. Show, S. H. Wang, G. M. Swain, *J. Electrochem. Soc.* **2005**, *152*, E184.
- [233] N. Rajalakshmi, K. S. Dhathathreyan, *Int. J. Hydrogen Energy* **2008**, *33*, 5672.
- [234] O. Antoine, R. Durand, *Electrochem. Solid State Lett.* **2001**, *4*, A55.
- [235] T. J. Schmidt, U. A. Paulus, H. A. Gasteiger, R. J. Behm, *J. Electroanal. Chem.* **2001**, *508*, 41.
- [236] M. Lai, D. J. Riley, *J. Colloid Interface Sci.* **2008**, *323*, 203.
- [237] Y. G. Guo, J. S. Hu, H. M. Zhang, H. P. Liang, L. J. Wan, C. L. Bai, *Adv. Mater.* **2005**, *17*, 746.
- [238] P. N. Bartlett, J. J. Baumberg, P. R. Birkin, M. A. Ghanem, M. C. Netti, *Chem. Mater.* **2002**, *14*, 2199.
- [239] P. N. Bartlett, P. R. Birkin, M. A. Ghanem, *Chem. Commun.* **2000**, 1671.
- [240] S. H. Yoo, L. Liu, S. Park, *J. Colloid Interface Sci.* **2009**, *339*, 183.
- [241] W. Lee, M. Alexe, K. Nielsch, U. Gosele, *Chem. Mater.* **2005**, *17*, 3325.
- [242] B. Mayers, X. C. Jiang, D. Sunderland, B. Cattle, Y. N. Xia, *J. Amer. Chem. Soc.* **2003**, *125*, 13364.
- [243] V. V. Gulians, M. A. Carreon, Y. S. Lin, *J. Membr. Sci.* **2004**, *235*, 53.
- [244] F. C. Meldrum, R. Seshadri, *Chem. Commun.* **2000**, 29.
- [245] C. H. Cui, H. H. Li, S. H. Yu, *Chem. Commun.* **2010**, 46, 940.
- [246] T. Y. Shin, S. H. Yoo, S. Park, *Chem. Mater.* **2008**, *20*, 5682.
- [247] S. H. Yoo, S. Park, *Adv. Mater.* **2007**, *19*, 1612.
- [248] D. F. Acevedo, H. J. Salavagione, A. F. Lasagni, E. Morallon, F. Mucklich, C. Barbero, *ACS Appl. Mater. Interfaces* **2009**, *1*, 549.
- [249] G. S. Attard, P. N. Bartlett, N. R. B. Coleman, J. M. Elliott, J. R. Owen, J. H. Wang, *Science* **1997**, *278*, 838.
- [250] J. M. Elliott, P. R. Birkin, P. N. Bartlett, G. S. Attard, *Langmuir* **1999**, *15*, 7411.
- [251] S. Daniele, S. Bergamin, *Electrochem. Commun.* **2007**, *9*, 1388.
- [252] R. McGorty, J. Fung, D. Kaz, V. N. Manoharan, *Mater. Today* **2010**, *13*, 34.
- [253] T. M. Blattler, A. Binkert, M. Zimmermann, M. Textor, J. Voros, E. Reimhult, *Nanotechnology* **2008**, *19*.
- [254] Z. Z. Gu, A. Fujishima, O. Sato, *Chem. Mater.* **2002**, *14*, 760.
- [255] P. Ferreira-Aparicio, M. A. Folgado, L. Daza, *J. Power Sources* **2009**, *192*, 57.
- [256] J. Wang, D. F. Thomas, A. Chen, *Anal. Chem.* **2008**, *80*, 997.
- [257] K. Koczur, Q. F. Yi, A. C. Chen, *Adv. Mater.* **2007**, *19*, 2648.
- [258] Q. F. Yi, L. Li, W. Q. Yu, Z. H. Zhou, X. P. Liu, G. R. Xu, *J. Alloys Compd.* **2008**, *466*, 52.
- [259] Y. Luo, S. K. Lee, H. Hofmeister, M. Steinhart, U. Gosele, *Nano Lett.* **2004**, *4*, 143.
- [260] M. Steinhart, R. B. Wehrspohn, U. Gosele, J. H. Wendorff, *Angew. Chem., Int. Ed.* **2004**, *43*, 1334.
- [261] M. Mohl, A. Kumar, A. L. M. Reddy, A. Kukovec, Z. Konya, I. Kiricsi, R. Vajtai, P. M. Ajayan, *J. Phys. Chem. C* **2010**, *114*, 389.
- [262] L. Liu, S. H. Yoo, S. Park, *Chem. Mater.* **2010**, *22*, 2681.
- [263] Y. Y. Song, Z. D. Gao, J. J. Kelly, X. H. Xia, *Electrochem. Solid State Lett.* **2005**, *8*, C148.
- [264] C. Chen, J. Loo, M. Deng, R. Kox, R. Huys, C. Bartic, G. Maes, G. Borghs, *J. Phys. Chem. C* **2009**, *113*, 5472.
- [265] K. Tammeveski, T. Kikas, T. Tenno, L. Niinisto, *Sens. Actuators, B* **1998**, *47*, 21.
- [266] R. Lo Nigro, G. Malandrino, P. Fiorenza, I. L. Fragala, *ACS Nano* **2007**, *1*, 183.
- [267] H. Lechtman, *Technology and Culture* **1984**, *25*, 1.
- [268] Y. Ding, Y. J. Kim, J. Erlebacher, *Adv. Mater.* **2004**, *16*, 1897.
- [269] Z. C. Liu, S. Koh, C. F. Yu, P. Strasser, *J. Electrochem. Soc.* **2007**, *154*, B1192.
- [270] D. V. Pugh, A. Dursun, S. G. Corcoran, *J. Mater. Res.* **2003**, *18*, 216.
- [271] J. Erlebacher, M. J. Aziz, A. Karma, N. Dimitrov, K. Sieradzki, *Nature* **2001**, *410*, 450.
- [272] D. V. Pugh, A. Dursun, S. G. Corcoran, *J. Electrochem. Soc.* **2005**, *152*, B455–B459.
- [273] H. J. Jin, D. Kramer, Y. Ivanisenko, J. Weissmuller, *Adv. Eng. Mater.* **2007**, *9*, 849.
- [274] Z. H. Zhang, Y. Wang, Z. Qi, W. H. Zhang, J. Y. Qin, J. Frenzel, *J. Phys. Chem. C* **2009**, *113*, 12629.
- [275] S. Kerzenmacher, M. Schroeder, R. Brämer, R. Zengerle, F. von Stetten, *J. Power Sources* **2010**, *195*, 6516.
- [276] U. Gebhardt, J. R. Rao, G. J. Richter, *J. Appl. Electrochem.* **1976**, *6*, 127.
- [277] J. C. Thorp, K. Sieradzki, L. Tang, P. A. Crozier, A. Misra, M. Nastasi, D. Mitlin, S. T. Picraux, *Appl. Phys. Lett.* **2006**, *88*.
- [278] A. Antoniou, D. Bhattacharya, J. K. Baldwin, P. Goodwin, M. Nastasi, S. T. Picraux, A. Misra, *Appl. Phys. Lett.* **2009**, *95*.
- [279] J. Snyder, P. Asanithi, A. B. Dalton, J. Erlebacher, *Adv. Mater.* **2008**, *20*, 4883.
- [280] C. X. Xu, R. Y. Wang, M. W. Chen, Y. Zhang, Y. Ding, *Phys. Chem. Chem. Phys.* **2010**, *12*, 239.
- [281] H. Q. Li, A. Misra, J. K. Baldwin, S. T. Picraux, *Appl. Phys. Lett.* **2009**, *95*.
- [282] J. T. Zhang, P. P. Liu, H. Y. Ma, Y. Ding, *J. Phys. Chem. C* **2007**, *111*, 10382.
- [283] R. W. Ertenberg, B. Andracka, Y. Takano, *Physica B* **2000**, *284*, 2022.
- [284] R. Z. Yang, J. Leisch, P. Strasser, M. F. Toney, *Chem. Mater.* **2010**, *22*, 4712.
- [285] J. Erlebacher, *J. Electrochem. Soc.* **2004**, *151*, C614.
- [286] S. Koh, P. Strasser, *J. Amer. Chem. Soc.* **2007**, *129*, 12624.
- [287] A. Dursun, D. V. Pugh, S. G. Corcoran, *Electrochem. Solid State Lett.* **2003**, *6*, B32.
- [288] C. X. Xu, J. X. Su, X. H. Xu, P. P. Liu, H. J. Zhao, F. Tian, Y. Ding, *J. Amer. Chem. Soc.* **2007**, *129*, 42.
- [289] S. Parida, D. Kramer, C. A. Volkert, H. Rosner, J. Erlebacher, J. Weissmuller, *Phys. Rev. Lett.* **2006**, *97*, 035504.
- [290] R. Li, K. Sieradzki, *Phys. Rev. Lett.* **1992**, *68*, 1168.
- [291] Y. Ding, J. Erlebacher, *J. Amer. Chem. Soc.* **2003**, *125*, 7772.
- [292] R. R. Adzic, J. Zhang, K. Sasaki, M. B. Vukmirovic, M. Shao, J. X. Wang, A. U. Nilekar, M. Mavrikakis, J. A. Valerio, F. Uribe, *Top. Catal.* **2007**, *46*, 249.
- [293] H. C. Shin, J. Dong, M. L. Liu, *Adv. Mater.* **2003**, *15*, 1610.
- [294] Y. Li, Y. Y. Song, C. Yang, X. H. Xia, *Electrochem. Commun.* **2007**, *9*, 981.

- [295] Y. P. Deng, W. Huang, X. Chen, Z. L. Li, *Electrochem. Commun.* **2008**, *10*, 810.
- [296] W. Huang, M. H. Wang, J. F. Zheng, Z. L. Li, *J. Phys. Chem. C* **2009**, *113*, 1800.
- [297] R. Y. Wang, C. Wang, W. B. Cai, Y. Ding, *Adv. Mater.* **2010**, *22*, 1845.
- [298] J. Lin-Cai, D. Pletcher, *J. Electroanal. Chem.* **1983**, *149*, 237.
- [299] K. Sasaki, J. X. Wang, H. Naohara, N. Marinkovic, K. More, H. Inada, R. R. Adzic, *Electrochim. Acta* **2010**, *55*, 2645.
- [300] B. Hammer, J. K. Nørskov, *Surf. Sci.* **1995**, *343*, 211.
- [301] J. Zhang, K. Sasaki, E. Sutter, R. R. Adzic, *Science* **2007**, *315*, 220.
- [302] A. Roudgar, A. Gross, *Surf. Sci.* **2004**, *559*, L180.
- [303] J. T. Zhang, H. Y. Ma, D. J. Zhang, P. P. Liu, F. Tian, Y. Ding, *Phys. Chem. Chem. Phys.* **2008**, *10*, 3250.
- [304] D. J. Guo, H. L. Li, *J. Electroanal. Chem.* **2004**, *573*, 197.
- [305] S. Szabo, *Int. Rev. Phys. Chem.* **1991**, *10*, 207.
- [306] A. J. Bard, I. Rubenstein, *Electroanalytical Chemistry: A Series of Advances*, Marcel Dekker Inc. **1999**.
- [307] S. R. Brankovic, J. X. Wang, R. R. Adzic, *Surf. Sci.* **2001**, *474*, L173–L179.
- [308] K. Sasaki, Y. Mo, J. X. Wang, M. Balasubramanian, F. Uribe, J. McBreen, R. R. Adzic, *Electrochim. Acta* **2003**, *48*, 3841.
- [309] H. Tang, J. H. Chen, M. Y. Wang, L. H. Nie, Y. F. Kuang, S. Z. Yao, *Appl. Catal., A* **2004**, *275*, 43.
- [310] B. I. Podlovchenko, U. E. Zhumaev, Y. M. Maksimov, *J. Electroanal. Chem.* **2011**, *651*, 30.
- [311] T. S. Mkwizu, M. K. Mathe, I. Cukrowski, *Langmuir* **2010**, *26*, 570.
- [312] S. Papadimitriou, S. Armyanov, E. Valova, A. Hubin, O. Steenhaut, E. Pavlidou, G. Kokkinidis, S. Sotiropoulos, *J. Phys. Chem. C* **2010**, *114*, 5217.
- [313] S. Papadimitriou, A. Tegou, E. Pavlidou, S. Armyanov, E. Valova, G. Kokkinidis, S. Sotiropoulos, *Electrochim. Acta* **2008**, *53*, 6559.
- [314] A. Tegou, S. Papadimitriou, E. Pavlidou, G. Kokkinidis, S. Sotiropoulos, *J. Electroanal. Chem.* **2007**, *608*, 67.
- [315] S. R. Brankovic, J. McBreen, R. R. Adzic, *J. Electroanal. Chem.* **2001**, *503*, 99.
- [316] S. R. Brankovic, J. X. Wang, Y. Zhu, R. Sabatini, J. McBreen, R. R. Adzic, *J. Electroanal. Chem.* **2002**, *524*, 231.
- [317] B. C. Du, Y. Y. Tong, *J. Phys. Chem. B* **2005**, *109*, 17775.
- [318] P. K. Shen, N. Chi, K. Y. Chan, D. L. Phillips, *Appl. Surf. Sci.* **2001**, *172*, 159.
- [319] S. Patra, J. Das, H. Yang, *Electrochim. Acta* **2009**, *54*, 3441.
- [320] P. Del Angel, J. M. Dominguez, G. Del Angel, J. A. Montoya, J. Capilla, E. Lamy-Pitara, J. Barbier, *Top. Catal.* **2002**, *18*, 183.
- [321] D. X. Cao, S. H. Bergens, *Electrochim. Acta* **2003**, *48*, 4021.
- [322] N. T. Nguyen, S. H. Chan, *J. Micromech. Microeng.* **2006**, *16*, R1–R12.